Multidecadal Evaluation of WRF Downscaling Capabilities over Western Australia in Simulating Rainfall and Temperature Extremes

JULIA ANDRYS AND THOMAS J. LYONS

State Centre of Excellence for Climate Change, Woodland and Forest Health, Murdoch University, Perth, Western Australia, Australia

JATIN KALA

The Australian Research Council Centre of Excellence for Climate System Science, and Climate Change Research Centre, University of New South Wales, Sydney, New South Wales, Australia

(Manuscript received 15 August 2014, in final form 31 October 2014)

ABSTRACT

The authors evaluate a 30-yr (1981–2010) Weather Research and Forecast (WRF) Model regional climate simulation over the southwest of Western Australia (SWWA), a region with a Mediterranean climate, using ERA-Interim boundary conditions. The analysis assesses the spatial and temporal characteristics of climate extremes, using a selection of climate indices, with an emphasis on metrics that are relevant for forestry and agricultural applications. Two nested domains at 10- and 5-km resolution are examined, with the higher-resolution simulation resolving convection explicitly. Simulation results are compared with a high-resolution, gridded observational dataset that provides daily rainfall, minimum temperatures, and maximum temperatures. Results show that, at both resolutions, the model is able to simulate the daily, seasonal, and annual variation of temperature and precipitation well, including extreme events. The higher-resolution domain displayed significant performance gains in simulating dry-season convective precipitation, rainfall around complex terrain, and the spatial distribution of frost conditions. The high-resolution domain was, however, influenced by grid-edge effects in the southwestern margin, which reduced the ability of the domain to represent frontal rainfall along the coastal region. On the basis of these results, the authors feel confident in using the WRF Model for regional climate simulations for the SWWA, including studies that focus on the spatial and temporal representation of climate extremes. This study provides a baseline climatological description at a high resolution that can be used for impact studies and will also provide a benchmark for climate simulations driven by general circulation models.

1. Introduction

Changes in climate extremes are of particular interest because of their disproportionately large influence on ecosystems, agriculture, and human health (Patz et al. 2005; Easterling et al. 2000). The southwest of Western Australia (SWWA) has been identified as a region that is acutely at risk of climatic change (Hughes 2003; Malcolm et al. 2006); there is limited knowledge on how these changes are likely to manifest at the regional scale, however, in particular with respect to extremes. Forestry and agriculture encapsulate the majority of the land use in the SWWA and contribute significantly to regional prosperity. For example, cereal crops, the largest agricultural sector in the state, contribute AUD 4.5 billion annually to the Western Australian economy (Varnas 2014). Understanding how these industries may be impacted by changes in climate extremes is critical for developing management strategies that will enable adaptation and preserve this prosperity.

Niu et al. (2014) reviewed the current understanding of plant responses to climate extremes, including heat waves, frost, drought, and flooding, and found that, while the response was not uniform between ecosystems, extreme events generally have a deleterious effect on plant productivity and survivability. The negative response to drought and heat stress for forests globally is supported by Allen et al. (2010) and Clifford et al. (2013). When examining forest mortality events in the SWWA, Evans and Lyons (2013) found that sudden

Corresponding author address: Julia Andrys, Murdoch University, 90 South St., Murdoch WA 6150, Australia.
E-mail: j.andrys@murdoch.edu.au

DOI: 10.1175/JAMC-D-14-0212.1

increases in the diurnal temperature range were a significant factor in forest-mortality events, whereas Brouwers et al. (2012) established that the combination of drier-than-average conditions followed by heat-wave events also led to an episode of widespread decline within the native forest. Because forest ecosystems have acclimated to the prevailing conditions, extreme events tend to cause damage to the biota by increasing stress on the vegetation, making it less able to withstand other stresses such as, for example, attacks by bark beetles (Williams et al. 2012).

The response of agricultural production, particularly cereal crops, to extreme conditions is more temporally dependent and is linked with the growing cycle. Frost or high temperatures that occur in the grain-filling period of the crop-growth cycle, for example, will result in the most significant reduction in agricultural yield (Asseng et al. 2012; Ludwig and Asseng 2006; Zheng et al. 2012). It is therefore clear that assessments of future changes in climate on agriculture and forestry need to focus on climate extremes, with a particular focus on the magnitude and timing of these events.

Investigating changes in extremes of both temperature and precipitation is difficult within the constructs of general circulation models (GCMs) because their resolution does not allow for the adequate representation of finer-scale features, including topography and land cover, and mesoscale weather systems, which play a significant role in the development of extreme conditions (Ekström et al. 2005; Fowler et al. 2005; Donat et al. 2010; Mishra et al. 2012). As such, downscaling techniques, including dynamical downscaling, are frequently applied to GCM output. The Weather Research and Forecasting (WRF) Model (Skamarock et al. 2008) employed as a regional climate model (RCM) is one such tool for this purpose. The ability of WRF to downscale GCMs and to better account for regional climate has been well established in simulations conducted over climatological regions in Europe (Christensen et al. 2007; Chu et al. 2010), North America (Mearns et al. 2009; Patricola and Cook 2013), and Asia (Chotamonsak et al. 2011). A number of these studies have also included an assessment of climate extremes (Argüeso et al. 2011; Gao et al. 2012; Salathé et al. 2010). To promote a consistent method for regional downscaling experiments and hence to improve the quality of experiment outcomes, the Coordinated Regional Downscaling Experiment (CORDEX; Giorgi et al. 2009) was established. The CORDEX framework highlights the importance of first validating the RCM configuration through the evaluation of simulations with boundary conditions derived from reanalysis data before simulations downscaling GCM data are run.

Kala et al. (2015) examined a number of physics options for WRF in the SWWA for a 12-month period and found that the model was sensitive to parameterization options, in particular the choice of longwave and shortwave radiation schemes, land surface model, and planetary boundary layer scheme. Kala et al. (2015) also found that at a 10-km resolution WRF was not able to represent the magnitude of dry-season rainfall, and a systematic underestimation of coastal precipitation was linked to unresolved topography in the region. The influence of unresolved topography on simulated precipitation is supported by regional climate studies in other regions, which have found that higher-resolution simulations represent precipitation with greater skill (Cardoso et al. 2013; Warrach-Sagi et al. 2013).

In this study we aim to validate WRF as an RCM in the SWWA that is forced by reanalysis data over a 30-yr period between 1981 and 2010. We evaluate the ability of WRF to simulate extremes of temperature and precipitation in the SWWA as the basis for ongoing research to downscale an ensemble of GCMs to examine the impact of future climate changes. To achieve this aim, we consider the extent to which increasing the resolution of the WRF simulation will improve simulation of extremes. The ability of the simulation to detect the daily, seasonal, and annual variability of the SWWA is evaluated to ensure that WRF can adequately represent the climatological characteristics of the region. The spatial and temporal distribution of some extreme precipitation and temperature indices are also assessed.

2. Methods

a. Southwest Western Australia

SWWA is a region of high biological diversity (Fitzpatrick et al. 2008), which also supports an urban population in the coastal city of Perth and extensive rainfed cereal crops toward the interior. The growing season for these crops is in the cooler months of May–October (Ludwig and Asseng 2006). In the region, summer is from December to February (DJF), autumn is from March to May (MAM), winter is from July to August (JJA), and spring is from September to November (SON). SWWA experiences hot dry summers and cool wet winters, typical of its Mediterranean-type climate (Gentilli 1971, 108–114), but this type of climate in combination with low soil fertility means that the biota and agricultural resources of the region are highly susceptible to changes in climate (Kingwell 2006).

The most influential large-scale driver of the SWWA climate is the position of the subtropical high pressure

belt (Gentilli 1971, 108–114). In the spring and summer, the belt is positioned to the south of SWWA and advects hot continental air to the coast while channeling the passage of rain-bearing frontal systems to the south, resulting in dry conditions. Summer rainfall is a result of surface convection, cutoff lows (Pook et al. 2012), and northwesterly cloud bands that bring rain to the interior (Tapp and Barrell 1984). Infrequent, large-scale summer rain events in the SWWA, which occur only two or three times in a decade, were described by Wright (1974). Caused by meridional troughs passing over the region, Wright (1974) found that these rain events often took place when a former tropical cyclone was present north of Western Australia. Previous studies assessing WRF downscaling capabilities over the SWWA on a seasonal time scale have found that the scarcity and distribution of rain in the summer months is challenging to represent accurately (Kala et al. 2015). In the winter months the subtropical high pressure belt moves northward, allowing for the passage of frontal systems over the region that are the main source of annual rainfall. Annual rainfall variability in the region is considerable (Power et al. 1998) and has been found to be influenced by large-scale teleconnections, such as the Indian Ocean dipole (England et al. 2006).

SWWA is an area of low relief. The main topographical feature that influences the climate of the region is the Darling Scarp, which runs parallel to the coast 25 km inland and results in a sudden change in elevation of approximately 300 m. This feature can be seen in Fig. 1b. The meteorological influence of this scarp has been shown to be difficult to represent in mesoscale models with resolutions that are more coarse than 0.5 km (Pitts and Lyons 1990; Kala et al. 2011, 2015).

b. *Model configuration*

A 30-yr, three-domain regional climate simulation from 1981 to 2010 was conducted using WRF, version 3.3, driven by ERA-Interim (Dee et al. 2011) boundary conditions. A 3-month model spinup period was used. The outer 50-km domain (Fig. 1a) was based on the CORDEX Australia domain. The two nested domains, at 10- and 5-km resolution, were chosen to evaluate the influence of spatial scale on model skill and also to compare the performance of parameterized convection with convection that is explicitly resolved in the model. We note that the downscaling ratio of 2 used between our two nested domains is a lower ratio than is usually employed by regional climate simulations. Our choice of downscaling ratio between these domains was based on the limits of the computational resources available. This meant that the resolution of the inner domain (5 km) matched the resolution of the gridded observational dataset, which is discussed in section 2c.

Parameterization options and model setup were based on the findings of a prior sensitivity analysis of WRF to different physics and input data over SWWA (Kala et al. 2015) and include the single-moment 5-class microphysics scheme (Hong et al. 2004), RRTM for longwave radiation (Mlawer et al. 1997), Dudhia shortwave radiation (Dudhia 1989), Yonsei University planetary boundary layer scheme (Hong and Lim 2006), convective parameterization on the first and second domains only from Kain–Fritsch (Kain 2004), the MM5 surface-layer scheme (Grell et al. 2000), and the Noah land surface model (Chen and Dudhia 2001). (Acronym definitions can be found at http://www.ametsoc.org/PubsAcronymList.) The model employs 30 vertical levels, which are more densely spaced near the surface, 150-day averaging for deep soil temperatures, and spectral nudging for the upper layers of the outer domain only. Carbon dioxide concentrations were updated on a monthly frequency on the basis of observations from Baring Head, New Zealand (Keeling et al. 2001), as being representative of the Southern Hemisphere. A 10-gridpoint relaxation zone was removed from the domain boundaries prior to analysis of the results.

c. *Observational data*

Observational data used for evaluation come from a daily gridded dataset of maximum and minimum temperatures and rainfall provided by the Australian Bureau of Meteorology (BoM) as a contribution to the Australian Soil Water Availability Project (AWAP; Raupach et al. 2009). The AWAP temperature and precipitation dataset, at a resolution of 5 km, is an interpolation from a network of weather stations across Australia (Jones et al. 2009) and has been used as a validation tool for previous regional climate simulations in Australia (Evans and McCabe 2010; Evans et al. 2012; Kala et al. 2015). We note the uncertainties associated with the fitting of surfaces to the observations to yield the gridded dataset, but the AWAP data have employed topography-resolving analysis methods to minimize this uncertainty (Jones et al. 2009). King et al. (2013) evaluated the merits of the AWAP dataset to examine extreme-rainfall characteristics and found that it demonstrated good agreement with station data and was suitable to examine extreme rainfall. King et al. (2013) did suggest caution in using the AWAP data in areas of low station density, but these regions are sufficiently removed from the two innermost domains of this simulation so as not to influence the quality of the observational data for this study. The AWAP data are

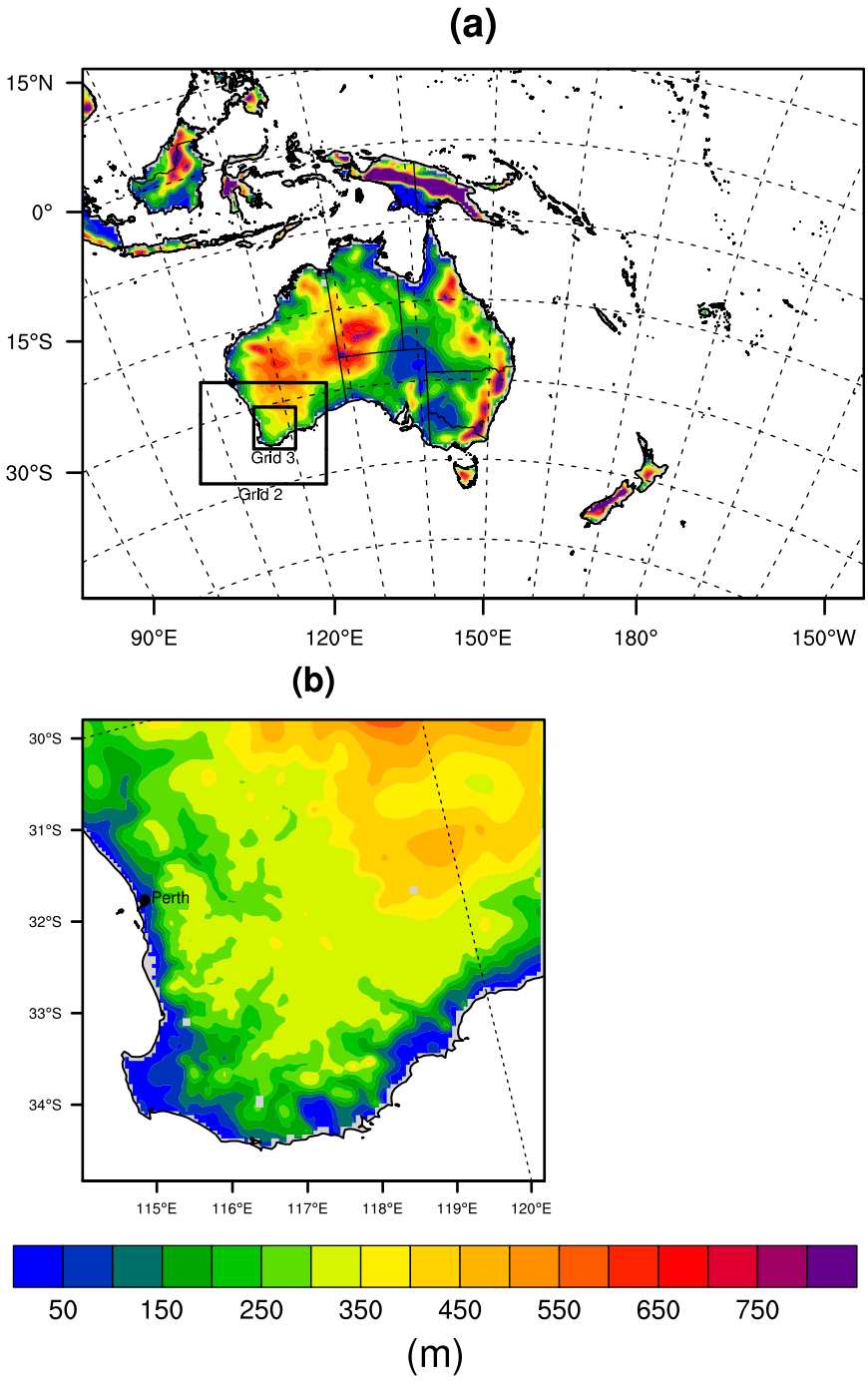

FIG. 1. RCM terrain for the (a) outer model domain, including the extent of the nested grids, and (b) the higher-resolution terrain of domain 3.

illustrated in Fig. 2, which shows the average seasonal mean rainfall, maximum temperatures, and minimum temperatures for 1981–2010. Precipitation (Fig. 2c) is most heavily concentrated at the coast, and there is a significant decline in rainfall as distance inland increases.

d. Statistics and indices

The AWAP observations were interpolated using simple inverse-distance weighting to the 5- (W5k) and 10-km (W10k) domains to enable intercomparison. Daily variability was quantified using probability density

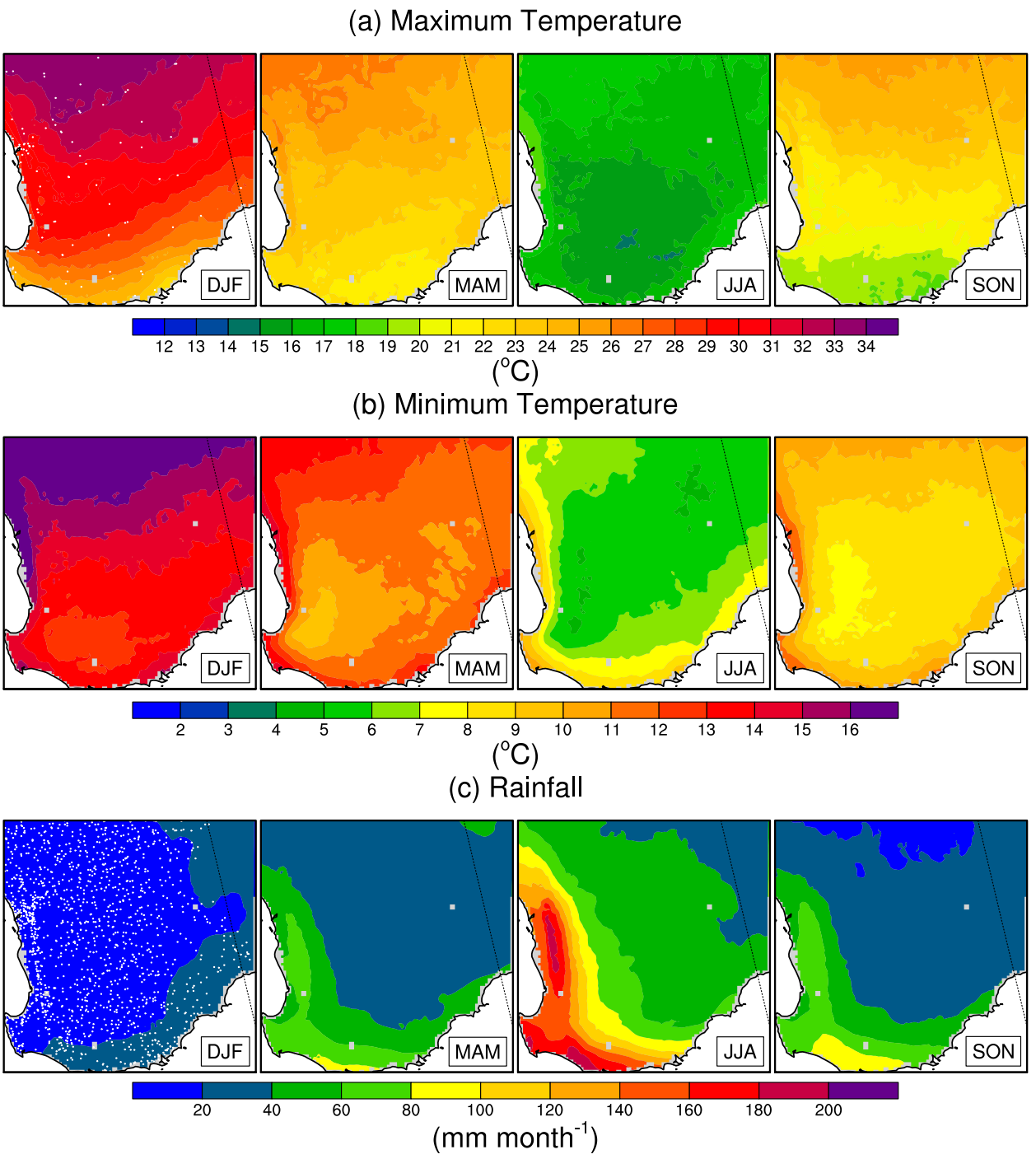

FIG. 2. Climatological seasonal means of AWAP (a) maximum temperatures, (b) minimum temperatures, and (c) rainfall for the W5k domain. The stations that have been used to generate the AWAP dataset are shown as white dots on the DJF plots in (a) for temperature and (c) for precipitation.

functions (PDFs). Because the observational data do not include daily rainfall values of less than 0.2 mm, simulation values below this threshold have been removed from the daily variability analysis. To establish the spatial variability of the daily PDFs, the Perkins skill score (PSS; Perkins et al. 2007) was employed, which compares the observed and simulated probability distributions:

$$\mathrm{PSS} = \sum_{1}^{n} \mathrm{minimum}(z_s, z_o), \tag{1}$$

where n is the number of bins used to calculate the PDF, z_s is the simulated frequency of values in n, and z_o is the observed frequency of values in n. Perfect agreement between the PDFs will result in a PSS of 1. If the model represents the observed PDF poorly, there will be less of an overlap between the two distributions and the PSS will be close to 0.

Simulation skill in representing the seasonal spatial variability of temperature and rainfall was assessed through the use of Taylor diagrams (Taylor 2001) and bias contour plots. WRF's ability to reproduce the interannual climatic variability of the SWWA is examined using annual time series plots of regionally averaged minimum and maximum temperature anomalies. Interannual variability with respect to precipitation was examined by plotting a time series of the regionally averaged annual precipitation anomaly.

We assessed the ability of WRF to represent aspects of temperature and precipitation extremes by using a number of the core indices developed by the World Meteorological Organization working group, the Expert Team on Climate Change Detection and Indices (ETCCDI; Persson et al. 2007). Some of the indices applied in this paper have been modified to be more relevant to the proposed applications of this research. For example, the ETCCDI frost-days (FD) index provides an annual count of days on which minimum temperature is lower than 0°C. Kala et al. (2009), however, have shown that screen temperatures of less than 2°C are sufficient to result in foliage temperatures below 0°C and hence frost damage to crops in SWWA. Therefore we use the threshold of 2°C for FD. In addition, the summer-days (SU) index is an annual count of days on which temperatures exceed 25°C. In the SWWA, 25°C is more representative of a mean temperature rather than an extreme, and as such we have modified this index to a threshold of 34°C. This level is based on studies by Asseng et al. (2011) and Wardlaw (1994), who found that temperatures in excess of 34°C can have significant impact on grain yields, particularly in the reproductive and grain-filling stages of the crop cycle. We note that there are many other temperature-based indices defined by the ETCCDI that are based on percentiles; for the applications intended for this research, however, we felt that the threshold-based approach of the FD and SU indices was the most relevant.

The precipitation indices examined in this study are applied as defined by the ETCCDI, but for percentile-based indices we have used 1981–2010 as the baseline period. These include the 5-day maximum precipitation intensity (Rx5day):

$$\mathrm{Rx5day}_j = \max(\mathrm{RR}_{kj}) \tag{2}$$

(where RR_{kj} is the precipitation amount for the 5-day interval ending at k in period j), the simple daily intensity index (SDII):

$$\mathrm{SDII}_j = \frac{\sum_{w=1}^{w} \mathrm{RR}_{wj}}{W} \tag{3}$$

(where RR_{wj} is the daily precipitation amount on a wet day w when RR ≥ 1 mm in period j and W is the number of wet days in j), and the annual total precipitation for which rainfall exceeds the 95th percentile (R95pTOT):

$$\mathrm{R95pTOT}_j = \sum_{w=1}^{w} \mathrm{RR}_{wj}, \quad \text{where} \quad \mathrm{RR}_{wj} > \mathrm{RR}_{\mathrm{wn}}95, \tag{4}$$

(where RR_{wj} is the daily precipitation amount on a wet day w when RR ≥ 1 mm in period j and $\mathrm{RR}_{\mathrm{wn}}95$ is the 95th percentile of precipitation on wet days in the 1981–2010 normal period).

Although three domains were used, the analysis in this paper is restricted to the two inner nested domains over SWWA. The outer domain was chosen to conform to the CORDEX specifications so as to contribute to the CORDEX initiative. Although a thorough analysis of the outer domain would certainly be useful, it does not fit within the scope of this paper, which is to focus on the agricultural and forested regions of SWWA. Results from the outer CORDEX Australia domain will be the subject of a separate study.

3. Results

In this section, the WRF simulations are compared with the AWAP observations to evaluate the overall performance of the model and the relative performance of the two nested domains. To allow for direct comparison between W5k and W10k, the larger W10k domain has been limited to the extent of the W5k domain.

a. Precipitation

1) Daily rainfall

The domain-averaged PDF of observed and simulated daily rainfall is shown in Fig. 3a for W10K and Fig. 3b for W5k. The distribution highlights the prevalence of days with rainfall under 1 mm; this interval accounts for 55% of all rain days in the region. The overall distribution of

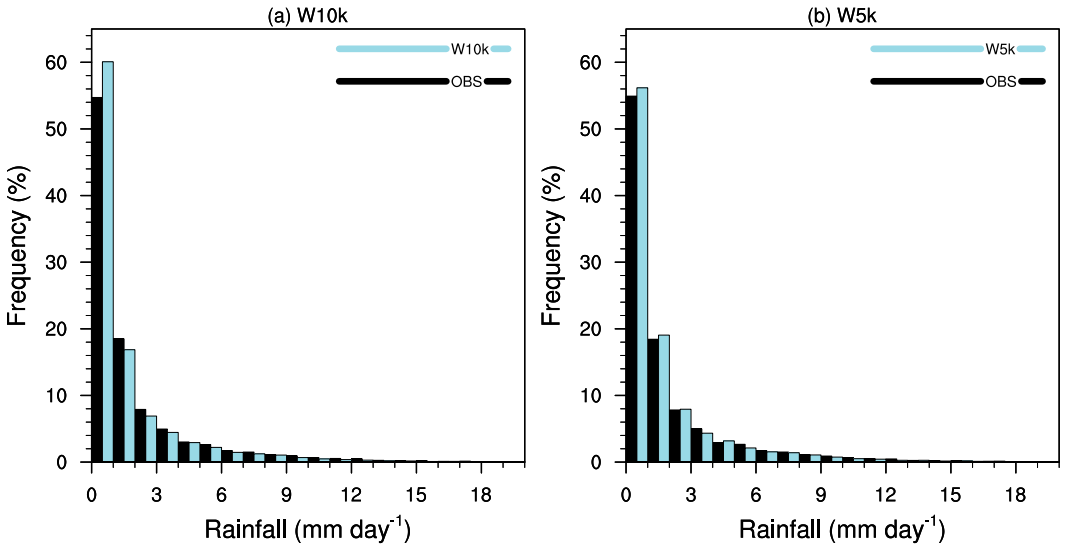

FIG. 3. Probability density plot of domain-averaged daily rainfall for (a) W10k and (b) W5k vs observations.

rainfall is simulated well, albeit with a tendency to overestimate the probability of light precipitation, particularly by W10k. This is apparent because W10k produced 4% more (59.74% as compared with 54.92%) days with rainfall below 1 mm than were observed. The overestimation of small precipitation events is improved by W5k, for which the proportion of days with less than 1 mm of rainfall is only 1.25% above observations. In their simulation over Portugal, the findings of Soares et al. (2012) closely match our own, specifically that WRF represents high-rainfall days well but tends to overestimate the proportion of days with low rainfall or drizzle. In a similar way, Soares et al. (2012) found that the higher-resolution simulation reduced the tendency for the model to simulate drizzle. Evans and McCabe (2010) performed a similar analysis for precipitation in a regional climate simulation over eastern Australia and also found that higher-intensity rainfall events were simulated well; the tendency for the simulation to overestimate drizzle was regionally dependent in that study, however. The performance of the W10k domain is sensitive to the threshold of the PDF, especially for low rainfall amounts; 33.5% of rainfall days in W10k had rainfall below 0.5 mm as compared with 26.9% for W5k and 27.2% for observations.

PSS results over the domain are shown in Fig. 4. Although the range of skill scores between W10k (0.78–0.96) and W5k (0.78–0.97) does not show any significant variation, the difference in their spatial distribution is marked; in W5k most of the domain has skill scores over 0.875, with small areas below this threshold being generally confined to the southwestern coastline. Conversely, the majority of the W10k domain has skill scores below 0.875. Domain-averaged rainfall PSS are 0.87 for W10k and 0.91 for W5k. These scores are comparable to the findings of previous studies that have employed the PSS for spatial analysis of daily rainfall distribution (Evans and McCabe 2010; Perkins et al. 2007; Argüeso et al. 2012). The spatial distribution of rainfall intensity shows a clear improvement in the level of agreement between W10k and W5k, which is not an unexpected result given the findings of previous studies in the SWWA that highlighted the need for higher-resolution simulations to more accurately represent rainfall in the region (Kala et al. 2015).

2) SEASONAL RAINFALL

Seasonal rainfall variability in the SWWA is driven by the movement of the subtropical high pressure belt. A preliminary analysis (not shown) of mean sea level pressure (MSLP) patterns from the outer domain showed that WRF was able to reproduce typical MSLP patterns for summer and winter as compared with the BoM MSLP analysis.

Rainfall model agreement is examined using Taylor diagrams. These plots allow a succinct comparison of models using the metrics of pattern correlation (corr), RMSE, and variance ratio. Strong model performance will be indicated by values that are close to the x axis and near the line that is labeled as REF (a 1:1 variance ratio). Figure 5 shows that pattern correlation is high—greater than 0.9 in almost all cases. The exceptions for W10k are in DJF (corr = 0.56) and MAM (corr = 0.77); those for W5k are in DJF (corr = 0.84). The nature of DJF and MAM rainfall in SWWA's Mediterranean climate is sparse, convective events of limited spatial extent.

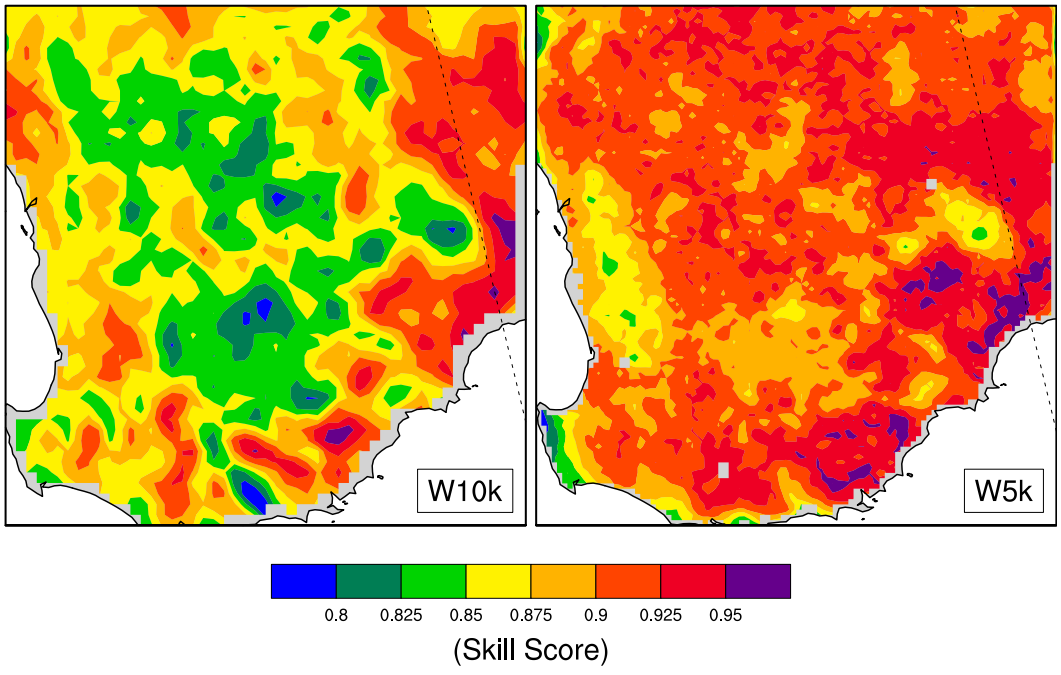

FIG. 4. PSS of daily precipitation for (a) W10k and (b) W5k.

Sparse, convective precipitation has been found by other studies (Soares et al. 2012; Kala et al. 2015) to be difficult for WRF to simulate well, particularly when using convective parameterization, and therefore the lower correlations we have seen for these two seasons are expected. The higher-resolution W5k simulation is able to improve performance with respect to the convective-dominated rainfall seasons (DJF and MAM) as a result of explicitly resolved convection and a higher-resolution domain, which can represent the patchy nature of this precipitation with greater skill. This is most significant in DJF, for which period the W5k simulation has improved W10k results from a pattern correlation of 0.55 to one of 0.84 and a variance ratio from 4.4 to 0.7. For the seasons of JJA and SON, for which rainfall in the SWWA is dominated by frontal systems, W5k deteriorates relative to the performance of W10k, especially with respect to the variance ratio, indicating that W5k is not capturing the variability of the rainfall in JJA and SON as well as W10k. This deterioration in JJA and SON rainfall variability for W5k can be explained by the strongly negative coastal winter rainfall biases in W5k, caused by domain-edge effects, which are discussed further in the following paragraphs.

Rainfall seasonal bias for both W10k and W5k is shown in Fig. 6. Across the region, and for all seasons except JJA, bias remains low and predominantly negative. JJA rainfall biases are considerably larger than in other seasons because most of the region's rainfall occurs in this season (Fig. 2c). Furthermore, the spatial distribution of bias shows a marked difference between W10k and W5k. W10k is producing a band of positive rainfall bias along the west coast of the region that is not present in the higher-resolution W5k. The area of positive bias in W10k aligns closely with the Darling Scarp, which runs parallel to the coast at this point (as shown in

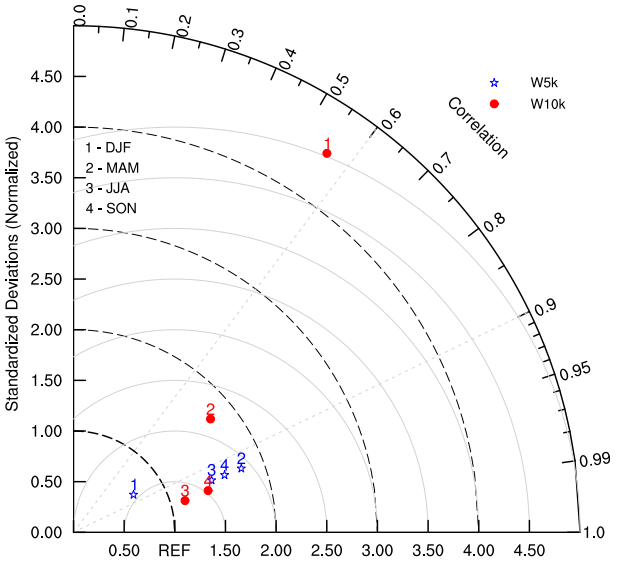

FIG. 5. Taylor plot showing seasonal rainfall performance for W10k (red) and W5k (blue).

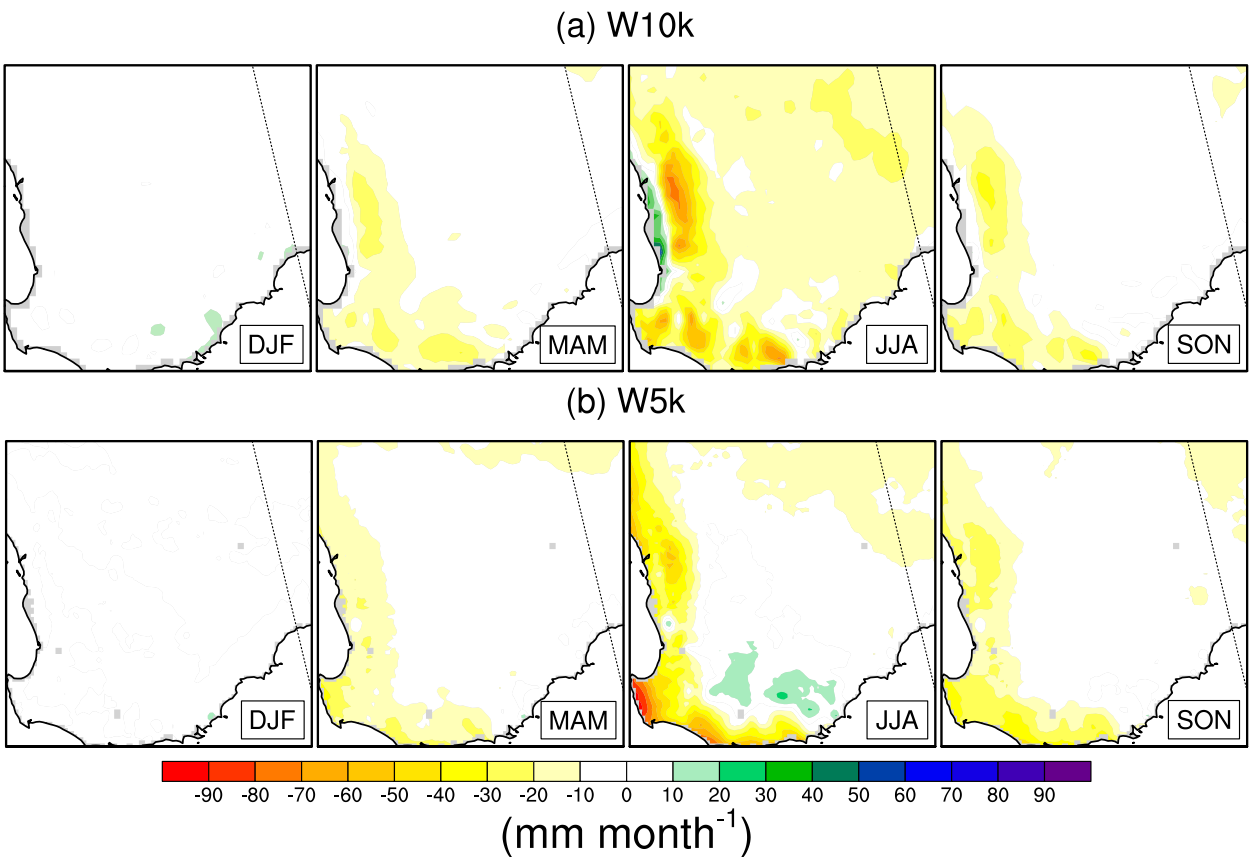

FIG. 6. Average seasonal rainfall bias (observation − simulation) for (a) W10k and (b) W5k.

Fig. 1b). The pattern of bias is consistent with the "windward/lee effect," in which mesoscale models tend to overestimate rainfall on the windward side of topographical features, as described by Wulfmeyer et al. (2008). In a 30-yr climate simulation over Germany, Warrach-Sagi et al. (2013) also found evidence of the windward/lee effect in WRF at 10-km resolution, but this error was overcome in short-run simulations at a convection-resolving scale (5 km). Consistent with Warrach-Sagi et al. (2013), W5k improves the representation of the Darling Scarp's influence on rainfall because W5k is able to eliminate the positive bias at the coast and much of the strong negative bias in the area to the east of the Darling Scarp. W5k is still showing an overall negative bias in this region, however, which suggests that the 5-km resolution is still not sufficient to fully resolve the meteorological influence of this topographical feature, which is supported by findings from Pitts and Lyons (1990) who found that representing the wind-generated turbulence of the scarp requires a 0.5-km resolution.

While the W5k simulation is overcoming the resolution-induced positive bias at the Darling Scarp, it is further enhancing the negative bias in the southwest corner of the region in JJA: up to 80 mm month^{-1}, which represents a relative error of approximately 60% of rainfall. To diagnose whether this bias could have resulted from grid-boundary interference, we considered the proximity of the area in question to the edge of the W5k grid. The southwest corner of the SWWA landmass begins 20 km (4 grid points) from the western boundary of the domain. A 10-gridpoint relaxation zone has been removed from this domain, but at 5-km resolution this represents a relaxation zone of only 50 km. It is therefore possible that this region is experiencing some anomalous rainfall output as a consequence of edge effects in this area interfering with the response of the model, as was found in Lowrey and Yang (2008) and Seth and Giorgi (1998).

A simulation (called W5k-ext) was run for the JJA period of 2007 (plus a 3-month spinup) with a 5-km domain extended to the south and west by 10 grid points to allow for further enhanced development of the frontal processes in this region away from the edge effects of the domain. This run was compared with a simulation initialized at the same time but using the standard 5-km

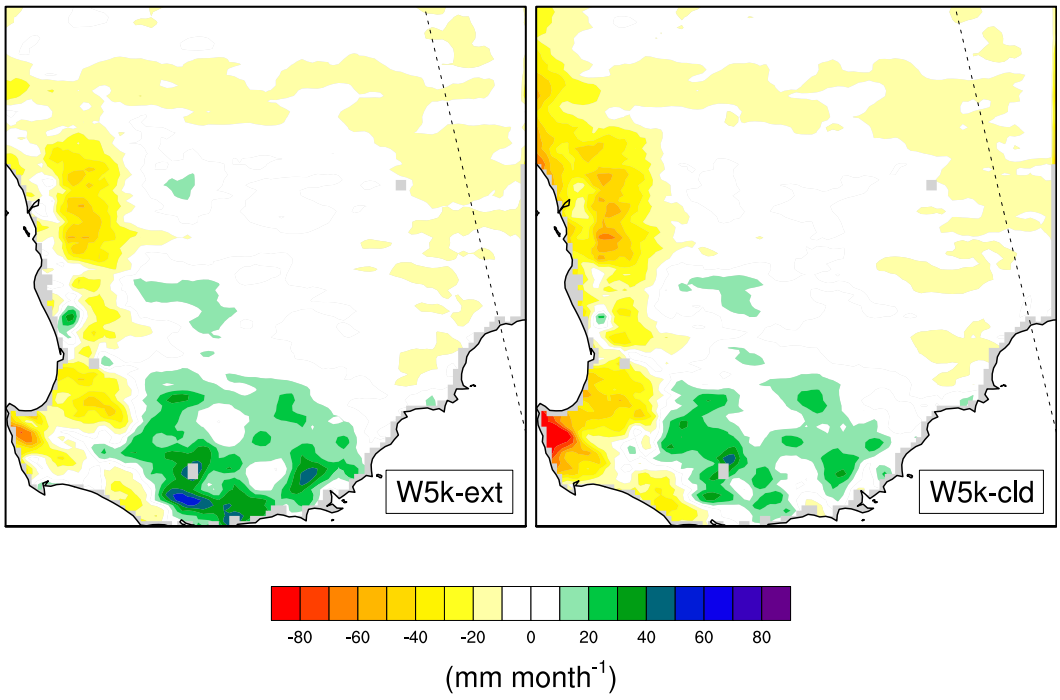

FIG. 7. Rainfall bias in JJA (2007) for (a) W5k-ext and (b) W5k-cld.

domain (called W5k-cld). The 2007 JJA season was chosen because the W5k simulation displayed the largest negative rainfall anomaly during this year. Bias plots for the 2007 JJA season are shown in Fig. 7, and it is apparent that the coastal bias has been reduced by the W5k-ext simulation; there has also been an increase in positive bias along the southern coastal region, however. We examined the individual rainfall events over the course of the W5k-ext simulation and found that this increased bias was systematic across all rainfall events. Identifying the physical mechanisms leading to this bias requires extra simulations with different domain setups, which will be the subject of future studies.

Notwithstanding, the overall marked reduction in bias provides a strong indication that the boundary proximity of the W5k domain is resulting in an anomalous rainfall response. Despite the reduction in bias, W5k-ext does still show a negative bias in the western coastal region, which indicates that the 5-km resolution is not fully resolving frontal processes. Kala et al. (2011) simulated the passage of cold fronts over the SWWA using a 5-km-resolution model. This study did not consider precipitation from these fronts at 5-km resolution (precipitation was examined at 20-km resolution only), but it did find that 5-km resolution was not sufficient to represent accurately the baroclinic zone at the frontal boundary, and we suggest that this smoothing of the baroclinic zone is contributing to the negative winter rainfall bias in W5k in the high-precipitation region of the southwest coast.

3) ANNUAL RAINFALL

Annual (December–November) precipitation anomalies for W10k and W5k are compared with observed precipitation anomalies in Fig. 8. Averaged over the region, the largest observed amplitude anomaly is $-200\,\mathrm{mm\,yr^{-1}}$ in 2010. There is little difference between the W10k and W5k simulations, which is likely due to averaging over the whole domain. In general, the simulations are able to account for the sign of the interannual variability well, particularly in the very low rainfall year of 2010, which was shown by Evans and Lyons (2013) to have resulted in a significantly increased number of forest-mortality events. There are exceptions in 1990, 2001, 2005, and 2007 in which the simulated precipitation anomaly was the opposite sign of the observed anomaly. The years 1990 and 2005 were wetter-than-average years that were simulated as being drier than average. The W5k DJF and JJA bias for these years is shown in Fig. 9a, and it is apparent that JJA bias follows a pattern that is similar to the climatological mean bias (Fig. 6) but that DJF rainfall is underestimated. Furthermore, 2001 and 2007 were drier-than-average years that were simulated as wetter than average. When the W5k DJF and JJA biases for these years are considered (Fig. 9b), JJA bias is again similar to the

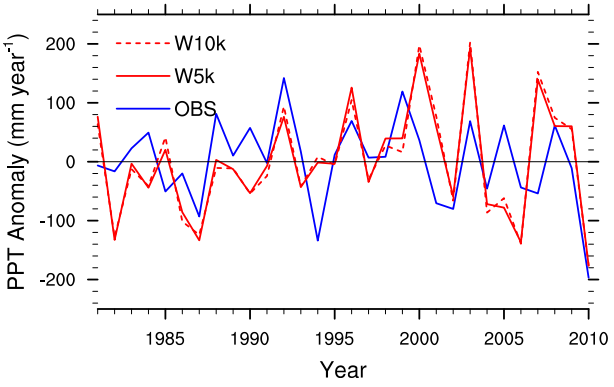

FIG. 8. Time series (1981–2010) of domain-averaged annual rainfall anomaly for observations (solid blue), W10k (dotted red), and W5k (solid red).

climatological mean, whereas DJF shows a very strong positive bias (W10k simulation bias is not shown because the pattern of bias closely matches that of W5k). This result indicates that simulation limitations with respect to dry-season rainfall events are the cause of the model's inability to detect the sign of the rainfall anomaly in these years.

To establish the source of the dry-season rainfall error, we considered the region's dry-season climatological behavior. Dry-season rainfall tends to be sporadic and sparse, but regional-scale rainfall events take place every 3–4 years on average. These events, triggered by high-level moisture advection from the tropics via meridional troughs, are simulated poorly by the model. Over the course of our simulation, 9 of these dry-season regional-scale rainfall events were observed. Our model generated 11 such events, 4 of which coincided with observed precipitation events in 2000, 2001, 2007, and 2008. Rainfall was overestimated for these events in both 2001 and 2007, leading to the anomalously high simulated mean rainfall in these years. Observed DJF rainfall in 1990 was also high as a result of a regional-scale rainfall event; this particular event was poorly simulated, however. The relatively low DJF bias seen in Fig. 6 shows that, over the 30-yr climatological period, the model is accounting for the extent of these regional-scale rainfall events well. When individual events are considered, however, the timing and magnitude are not well represented. We conducted a number of short simulations during 2007 with different initialization dates and found that the moisture-advection processes are particularly sensitive to the time since initialization, but there was no consistent pattern in this behavior. Further research is required to fully understand the nature of the misrepresentation of moisture advection within the outer domain of our model.

Figure 10 shows the spatial distribution of the standard deviation for annual rainfall. As expected, the largest observed variability is found in the highest-rainfall regions. Both W10k and W5k are able to represent the magnitude of the standard-deviation changes throughout the domain well. W5k is able to account for the spatial distribution of standard deviations better than W10k is in the midwest coastal region, but there is a large disparity between observations and W5k in the southwestern corner of the landmass that can be attributed to the grid-edge effects that are enhancing negative bias in this region.

4) EXTREME INDICES

We next examine indices that consider the contribution of rainfall from high-intensity events (R95pTOT and RX5day) and average rainfall intensity (SDII). From observations of SDII shown in Fig. 11a, it is apparent that the most intense rainfall is inland of the west coast, to the east of the Darling Scarp. W5k shows good spatial agreement with observations, especially in the area of highest precipitation intensity. SDII is underestimated by W5k in the southwest corner by approximately 2 mm day^{-1}. W10k represents the SDII as being the highest along the west coast, whereas the observations show that the highest-intensity rainfall occurs to the east of the Darling Scarp. The W10k representation of SDII is lacking in the finescale spatial structure of this index, which is well developed in W5k. W10k does, however, provide a better representation in the southwest corner and the interior of the domain than W5k does.

The RX5day index measures the highest annual rainfall in a 5-day period. Climatologically averaged annual RX5day is shown in Fig. 11b for the observations and for the W10k and W5K simulations. Similar to the SDII index, observations show that RX5day is highest in the region east of the Darling Scarp and along the southern coast, with declining intensity inland. Although there is spatial agreement for the W5k simulation, it is less well represented than the average intensity that was identified by the SDII index (Fig. 11). W10k does not capture the spatial pattern of Rx5day on the coast or in the Darling Scarp, and both W10k and W5k are overestimating RX5day in the interior.

The contribution of rainfall from the highest-intensity rainfall events (above the 95th percentile) is measured by the R95pTOT index. This metric differs from Rx5day because it considers all of the high-intensity rainfall events in a year over the percentile threshold whereas the RX5day only represents a single high-intensity event from each year. Observations for the R95pTOT index show a clear gradient from the southwest corner to the

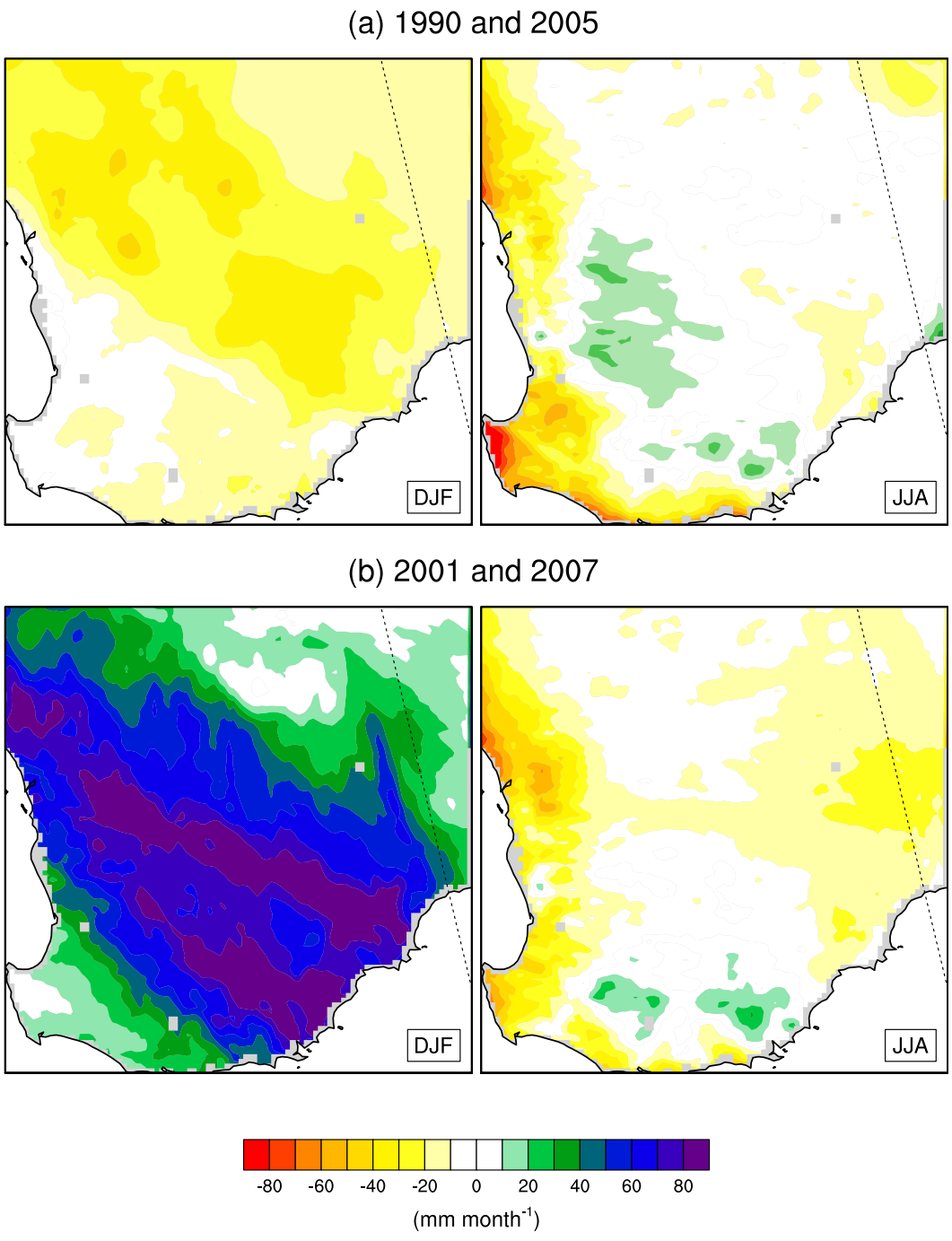

FIG. 9. Mean W5k (left) DJF and (right) JJA rainfall bias for (a) 1990 and 2005 and (b) 2001 and 2007.

northeast of the domain that is not as well defined in the W10k and W5k simulations (Fig. 11c). Both simulations show a significant departure from observations in the southwest corner, where the model is underestimating this index by over 100 mm (50%) in W5k and 50 mm (25%) in W10k. The W10k domain continues to miss the spatial distribution of the rainfall on the west coast; both W10k and W5k represent R95pTOT well over the interior of the SWWA, however. The RX5day and R95pTOT indices were evaluated by Argüeso et al. (2012) in a regional climate simulation over Spain. Their assessment of the performance of these metrics mirrors what we found here: the Rx5day index was well represented both spatially and with respect to magnitude and

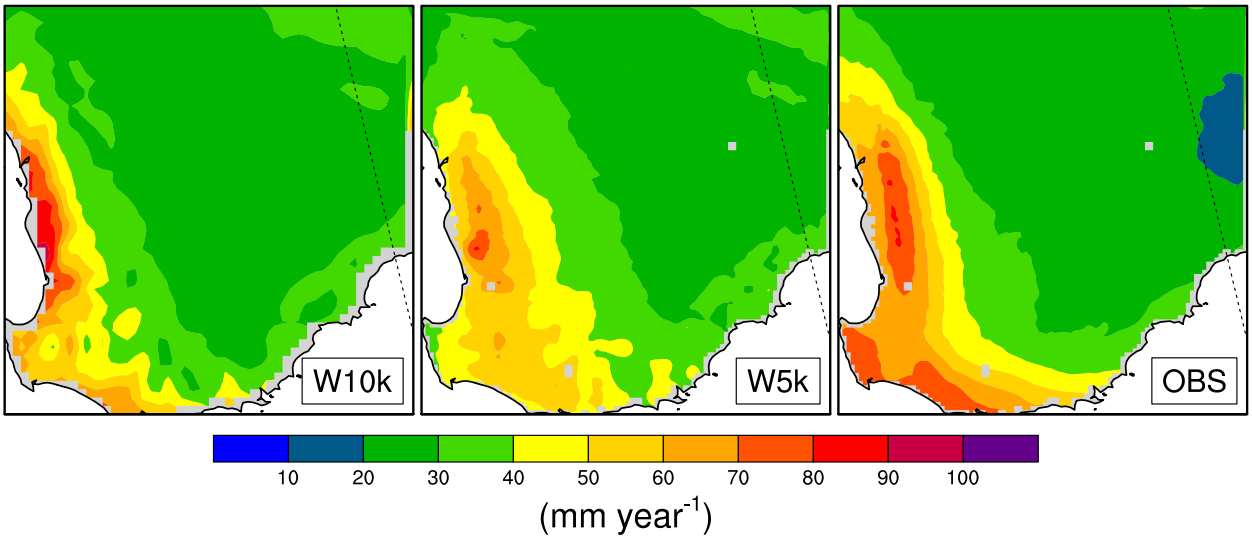

FIG. 10. Standard deviation of annual rainfall for W10k, W5k, and observations.

R95pTOT was less well matched, although broad spatial patterns were captured.

b. *Temperature*

1) DAILY TEMPERATURES

The PDFs of daily maximum and minimum temperatures for the 30-yr simulation comparing observations with both W10k and W5k are shown in Fig. 12. Domain-averaged PDFs for maximum temperatures show that the simulation distributions are skewed to the left, indicating that WRF is overestimating the proportion of cooler maximum temperatures. Temperatures toward the middle of the distribution are generally underestimated, and the extreme right of the distribution shows that the simulated hottest days closely match observations. This result suggests that, while moderate maximum temperatures tend to be underestimated and low maximum temperatures are overestimated, the occurrence of very hot maxima is well represented by the model. Critical for the applications of this research, the incidence of temperatures above 34°C shows good agreement; this is the threshold used by the SU index.

Conversely, the simulated distribution of minimum temperatures is skewed to the right, showing that the model is overestimating warm minima and underestimating the likelihood of moderately cold minima. An examination of the right tail of the W5k distribution (cold minima below 2°C) shows that the simulation corresponds to observations well; when minimum temperatures below 2°C are considered for the W10k distribution, however, there is a greater tendency to overestimate their frequency.

The goodness of fit of simulated PDFs relative to observations at each grid point is represented using the PSS in Fig. 13. The distribution of daily maximum and minimum temperatures is well represented in both the W10k and W5k simulations, with little difference apparent between the simulations. Mean PSS for minimum temperatures are equal (0.93) for both W10k and W5k simulations, and W10k (0.92) performs slightly better than W5k (0.91) for maximum temperatures. Maximum temperatures show their lowest levels of agreement on the southern coastal margins, where PSS values fall below 0.8.

2) SEASONAL TEMPERATURES

Figure 14 shows the mean seasonal performance of W10k and W5k maximum and minimum temperatures. Simulated maximum temperatures are represented well across all seasons and domains, with pattern correlation values between 0.9 and 1.0. Variance ratios are all below 1.0, which indicates that the spread of simulated seasonal mean temperatures was greater than observed. Both W10k and W5k show good representation of maximum temperatures, but results for W10k are somewhat better than for W5k, with generally higher pattern correlations and variance ratios that are closer to 1.0. Seasonal minimum temperatures are also represented well by the simulations; the pattern correlation values and variance ratios are lower than those of maximum temperatures, however—a finding that is consistent with similar regional climate simulations (Zhang et al. 2009; Soares et al. 2012). Unlike maximum temperatures, the W5k simulation is demonstrating better performance relative to W10k for seasonal minimum temperatures.

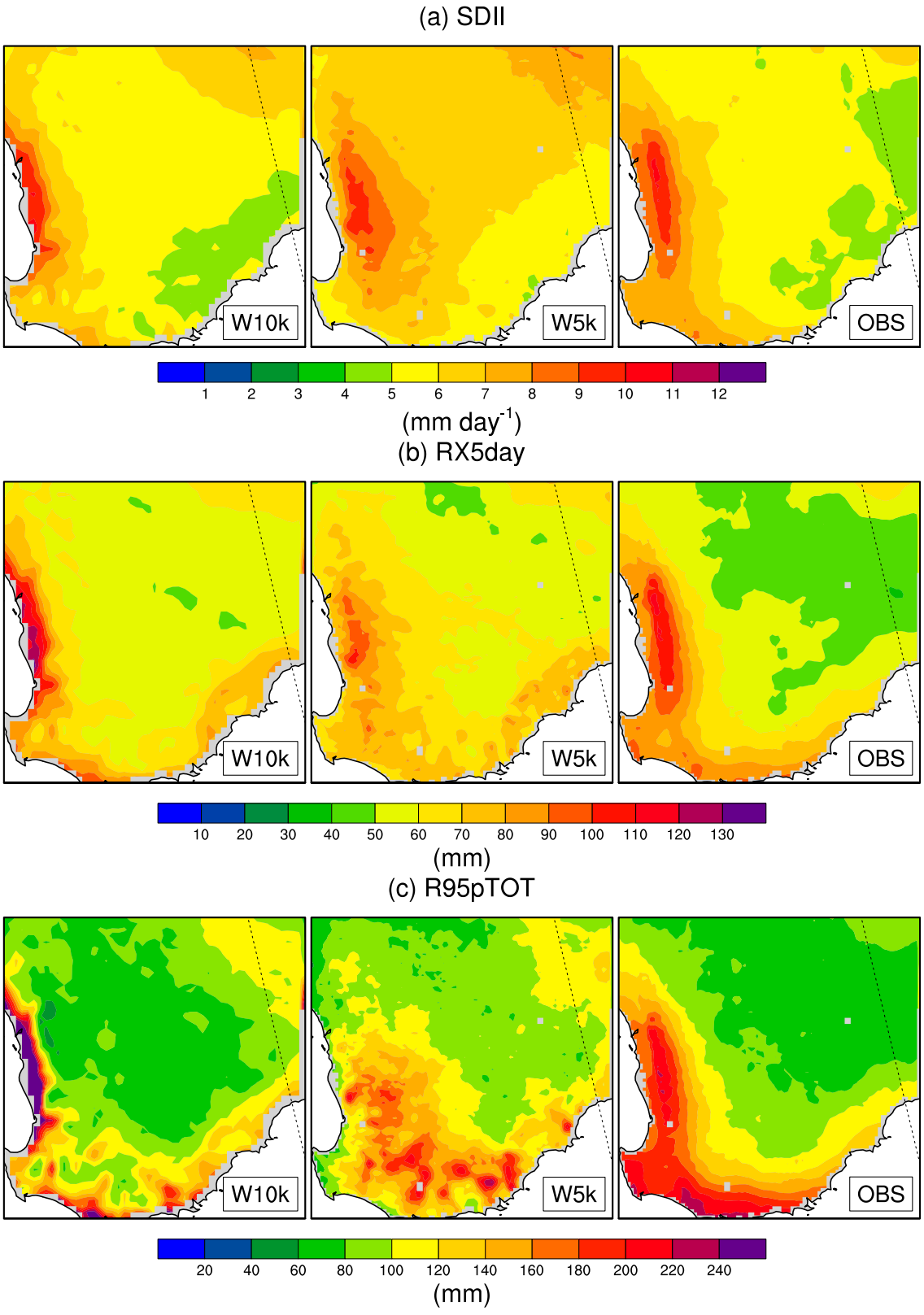

FIG. 11. Average values of annual precipitation indices (a) SDII, (b) RX5day, and (c) R95pTOT for W10k, W5k, and observations.

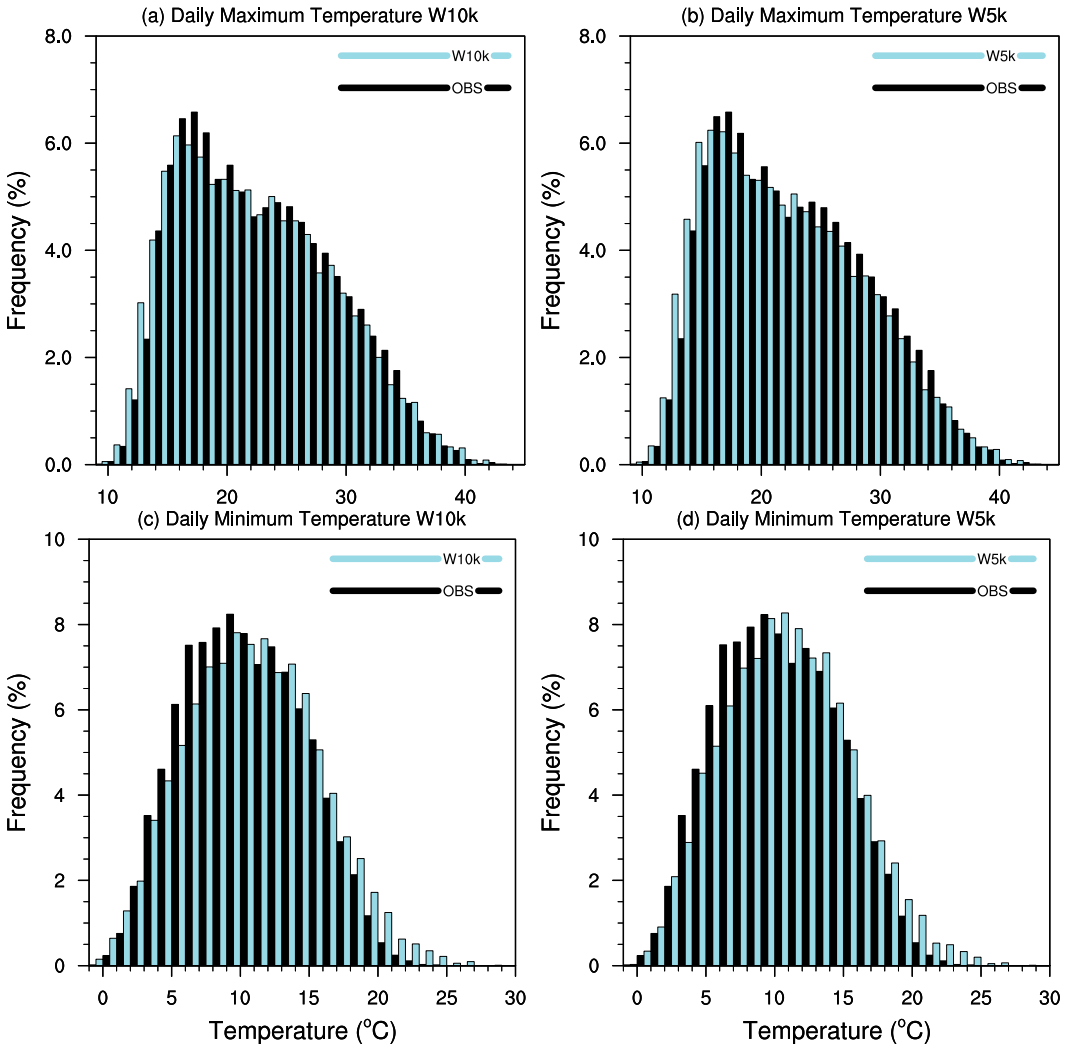

FIG. 12. Probability density plots comparing the distribution of daily maximum temperatures for (a) W10k and (b) W5k and minimum temperatures for (c) W10k and (d) W5k relative to observations.

The higher-resolution simulation (W5k) has more of a positive influence on minimum temperatures than on maximum temperatures because nighttime temperatures are more heavily influenced by local conditions, which are better represented in W5k.

Seasonal maximum temperature bias is shown in Figs. 15a and 15b. Temperatures display a systematic negative bias that is less than 2°C; in DJF this bias increases to −4°C along the southern coastal margin. This negative bias is intensified in the W5k simulation. Figures 15c and 15d show low biases for mean seasonal minimum temperatures in the W10k simulation (Fig. 15c) that are reduced further by the W5k simulation (Fig. 15d), with most of the study area having bias less than ±1°C. DJF and MAM show a slight increase in positive bias relative to JJA and SON; bias is relatively consistent across all seasons, however, which indicates that the model is able to account for seasonal changes in minimum temperatures in the SWWA well. There is a discernible and persistent warm bias for minimum temperatures over the Perth metropolitan area (the location of Perth is shown in Fig. 1b). This region represents the largest area of urban land use in the domain, and therefore a possible explanation for this bias is an unsuitable representation of the urban surface in the simulation (Chen et al. 2011). This simulation does not employ the use of an urban canopy model because the resolution of the simulation is too coarse to adequately resolve urban land use.

3) ANNUAL TEMPERATURES

Time series of domain-averaged annual minimum and maximum temperature anomalies are shown in Fig. 16.

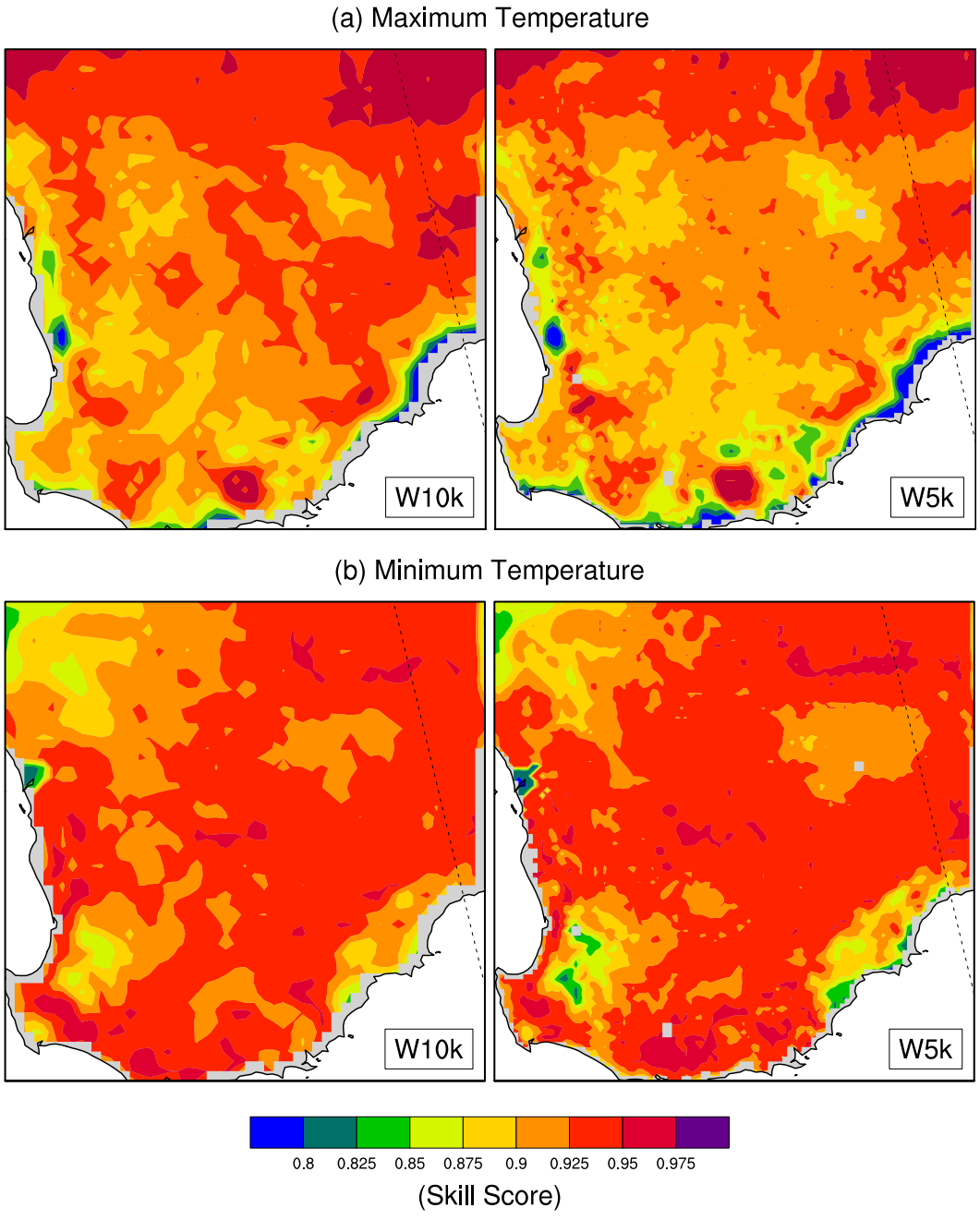

FIG. 13. PSS of (a) maximum temperature distributions and (b) minimum temperature distributions for (left) W10k and (right) W5k.

Over the duration of the simulation, observed temperature anomalies are small, less than ±1°C. These plots demonstrate that the simulations are able to reflect the interannual variations in temperature that are seen at the domain scale. This is especially true of minimum temperatures, for which the simulated anomalies are close to the observations. Simulated maximum temperatures show less skill in accounting for the observed variability. Although the magnitudes of the anomalies are well simulated over the 30-yr period, in 1984, 1987, 1998, 2001, 2003, and 2009 the sign of the temperature anomaly is poorly represented. The years 1984 and 1987 were colder-than-average years that were simulated as warmer than average. Conversely, 1998, 2001, 2003, and 2009 were warmer-than-average years but were simulated as colder than average. It was found

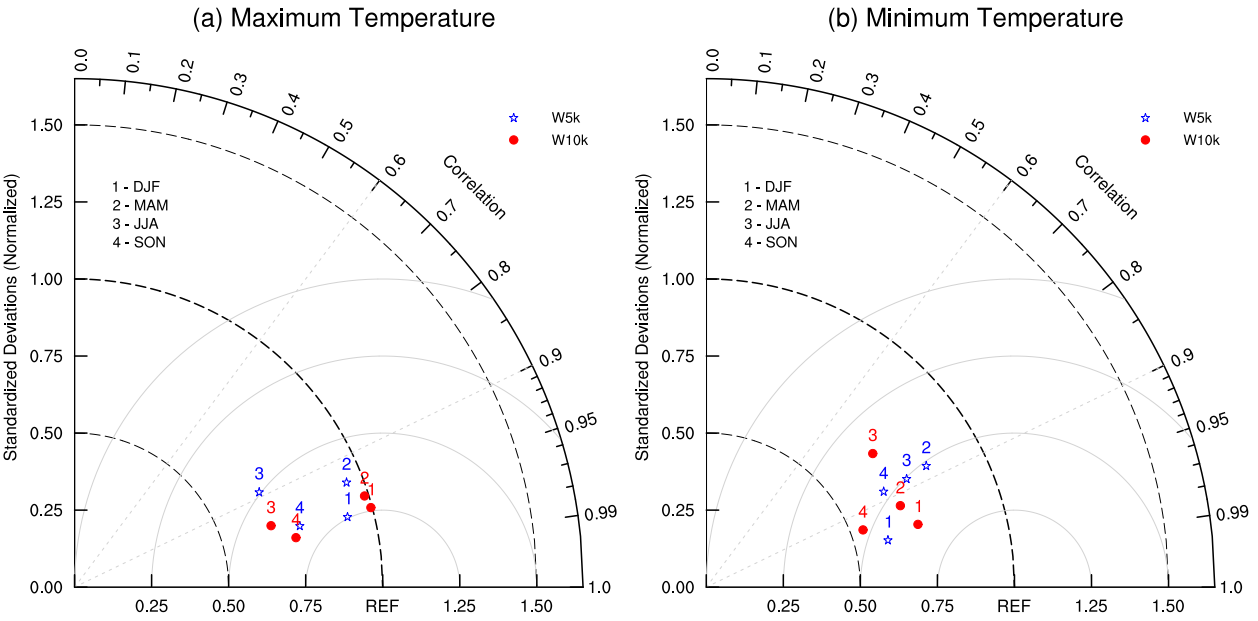

FIG. 14. Taylor plots showing the relative skill of W10k and W5k simulations for seasonal (a) maximum and (b) minimum temperatures.

that, similar to annual rainfall anomalies, these maximum temperature anomalies arise from fluctuations in the warm-season (DJF) biases, whereas the cooler-season (JJA) biases remain constant throughout the simulation. We considered whether these anomalous summer maximum temperature biases were linked with the model's poor simulation of regional-scale DJF rain events and could not find a consistent relationship with rainfall.

4) EXTREME INDICES

The FD index provides an annual count of days on which minimum temperatures are below 2°C. The climatologically averaged count of FD across the domain for W10k, W5k, and observations is shown in Fig. 17a. Observations highlight that the areas with the most FD are concentrated in the interior of the region and approximately 100 km inland of the western coastal margin. W10k and W5k show that the spatial extent of FD is represented well around the coastal regions. Both W10k and W5k overestimate the frost risk in the area to the east of the Darling Scarp and in the northwest corner of the domain, and FD is underestimated in the northeast. The higher-resolution W5k demonstrates a reduction in positive bias when compared with W10k. This improvement is enabled by the higher-resolution simulation allowing for more accurate representation of the local conditions, such as topography, that contribute to frost conditions.

Figure 17b illustrates the SU index. The simulated spatial representation of this index is overall satisfactory, and there is little difference between the two domains. This result is consistent with other studies that also found that maximum temperatures do not tend to be as heavily influenced as minimum temperatures are by increases in model resolution (Soares et al. 2012). There is an underestimation of the incidence of SU days in the north of the domain by approximately 5–10 days per year, which is a result of the negative bias in maximum temperatures that was found in the region (shown in Fig. 15).

The temporal characteristics of these temperature thresholds are very important, particularly how they interact with the cereal-crop growing season. As such, the mean monthly counts of these indices are now considered. Figure 18 shows that W10k and W5k are both able to represent the spatiotemporal development of FD in the growing season, with W5k showing an improved spatial representation and a reduction in positive bias. Simulations are demonstrating a small negative bias for early-season frost days (in May and June), showing that the model develops frost conditions later than observed; the spatiotemporal representation of frost is satisfactory, however.

Because the growing season is over the austral winter, the high-temperature threshold SU is exceeded less in the growing season than is FD. Figure 19 shows the monthly distribution of SU in those months that experience SU and highlights that the likelihood of SU in the growing season is low, with the north of the region experiencing less than 2 SU in October. Both W10k and W5k underestimate the extent of SU, but

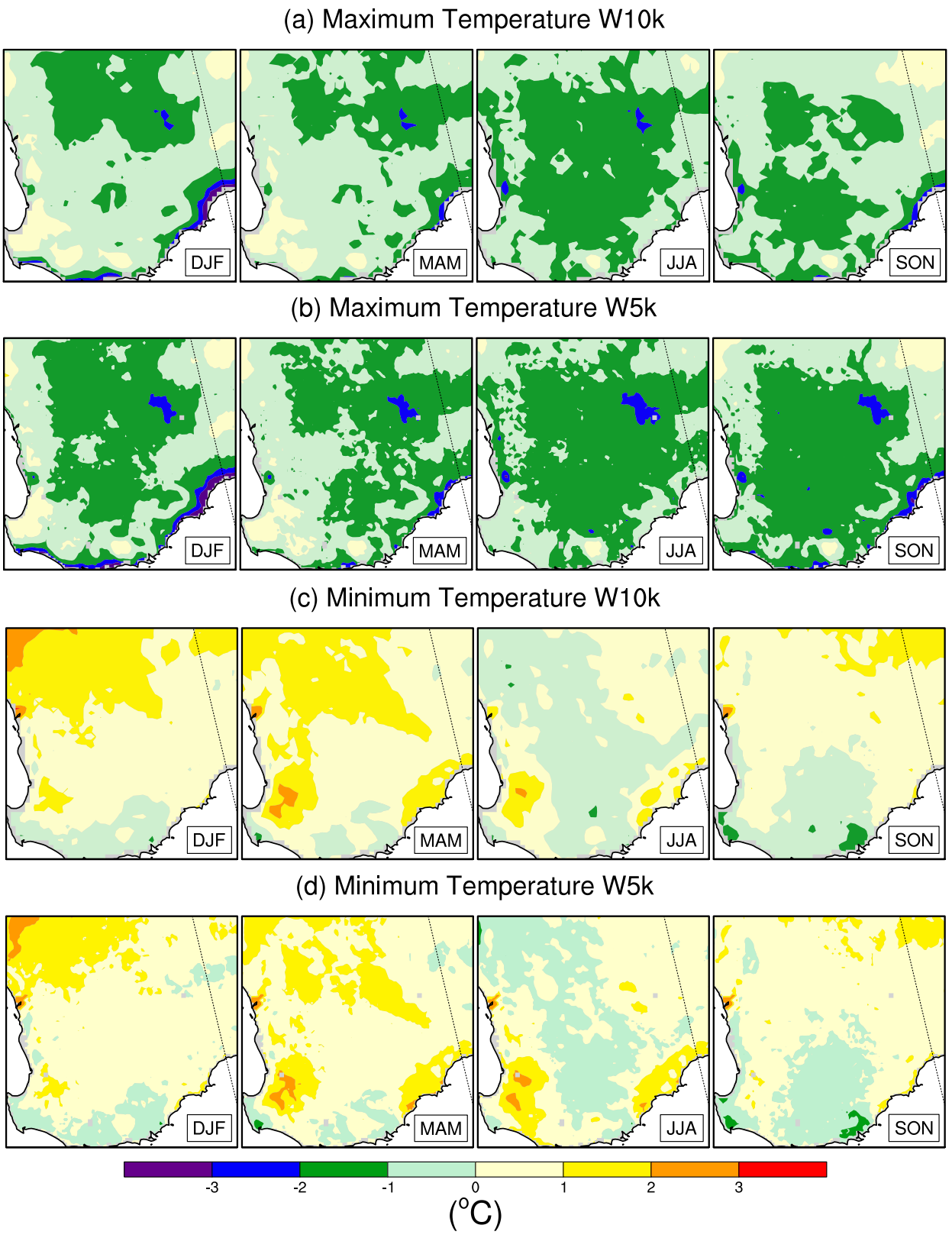

FIG. 15. Average seasonal temperature bias (observation − simulation) for (a) W10k maximum temperature, (b) W5k maximum temperature, (c) W10k minimum temperature, and (d) W5k minimum temperature.

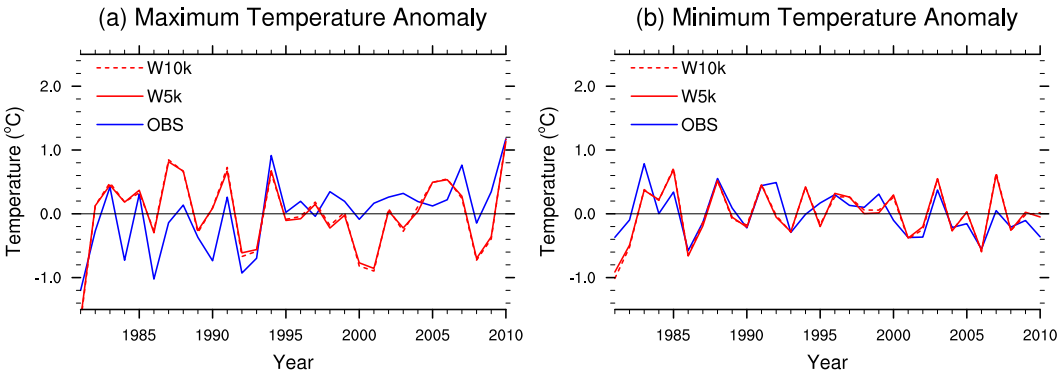

FIG. 16. Time series (1981–2010) of domain-averaged annual (a) maximum and (b) minimum temperature anomaly for observations (solid blue), W10k (dotted red), and W5k (solid red).

both simulations are able to account for the spatial distribution of monthly SU days, with W5k providing an improved representation of their magnitude relative to W10k.

4. Discussion and conclusions

We present an evaluation of the RCM WRF over the SWWA for 30 years between 1981 and 2010 to examine the ability of the model to accurately represent the ''climatology'' of the region, including the climatology of extreme events. Our study compared two domain resolutions: 10-km resolution using convective parameterization (W10k) and a 5-km domain that resolves convection explicitly (W5k).

Overall, we found that the simulation performed well in representing the climatology of the region. The statistical distribution of daily temperatures and rainfall showed that, while WRF tended to underestimate average maximum temperatures, warm extremes were well represented. This pattern was followed by rainfall, where daily high-intensity rainfall events were simulated well, and was mirrored by minimum temperatures, for which the mean was overestimated but very cold days showed good agreement with observations.

An analysis of seasonal variation showed that WRF was able to model seasonal minimum and maximum temperatures well. The W5k simulation improved the representation of minimum temperatures because of the improved resolution of local topographical effects but introduced additional bias for maximum temperatures. There were some large biases associated with JJA precipitation. While the positive bias on the midwest coast was overcome by W5k because of an improved topographical resolution of the Darling Scarp, the negative bias in the southwest corner was further enhanced. Bias in this region was influenced by the proximity of the grid edge to the coast in the W5k domain. This is indicated by a 3-month simulation for JJA in 2007 that showed that more than 50% of this bias was removed by expanding the W5k domain in a southerly and westerly direction. Even with the edge effects eliminated in the W5k-extended domain, a small negative bias on the southwest coast persisted. This follows the results from other studies in the SWWA that found that a 5-km resolution is not sufficient to fully resolve the baroclinic zone of the frontal systems that bring most of the JJA rainfall to the region (Kala et al. 2011). The W5k simulation was able to demonstrate significant improvements in the representation of DJF and MAM rainfall. Because of the edge effects that affect this simulation, it is not recommended that this domain be used for examining coastal precipitation, however. For future regional climate simulations it is strongly recommended that a larger domain, allowing for greater distance from the grid boundary to the coast, be used. The optimal spatial extent and positioning of the high-resolution domain relative to the coast is currently unknown, and further simulations will be required to establish how frontal rainfall processes are influenced by the location of the domain, as well as by horizontal and vertical resolution.

Extreme temperature indices were simulated well by WRF, especially by W5k, which was able to represent not only the magnitude but also the spatial and temporal distribution of FD and SU. Precipitation indices SDII, Rx5day, and R95pTOT were also modeled satisfactorily, but their performance was influenced by the biases found in both the W10k and W5k simulations. Soares et al. (2012) found that higher-resolution domains improved the simulation of precipitation extremes, and our results are not as conclusive in this respect. Note, however, that the Soares et al. (2012) highest-resolution domain was 9 km and used convective parameterization, comparable to our W10k domain. Furthermore, the

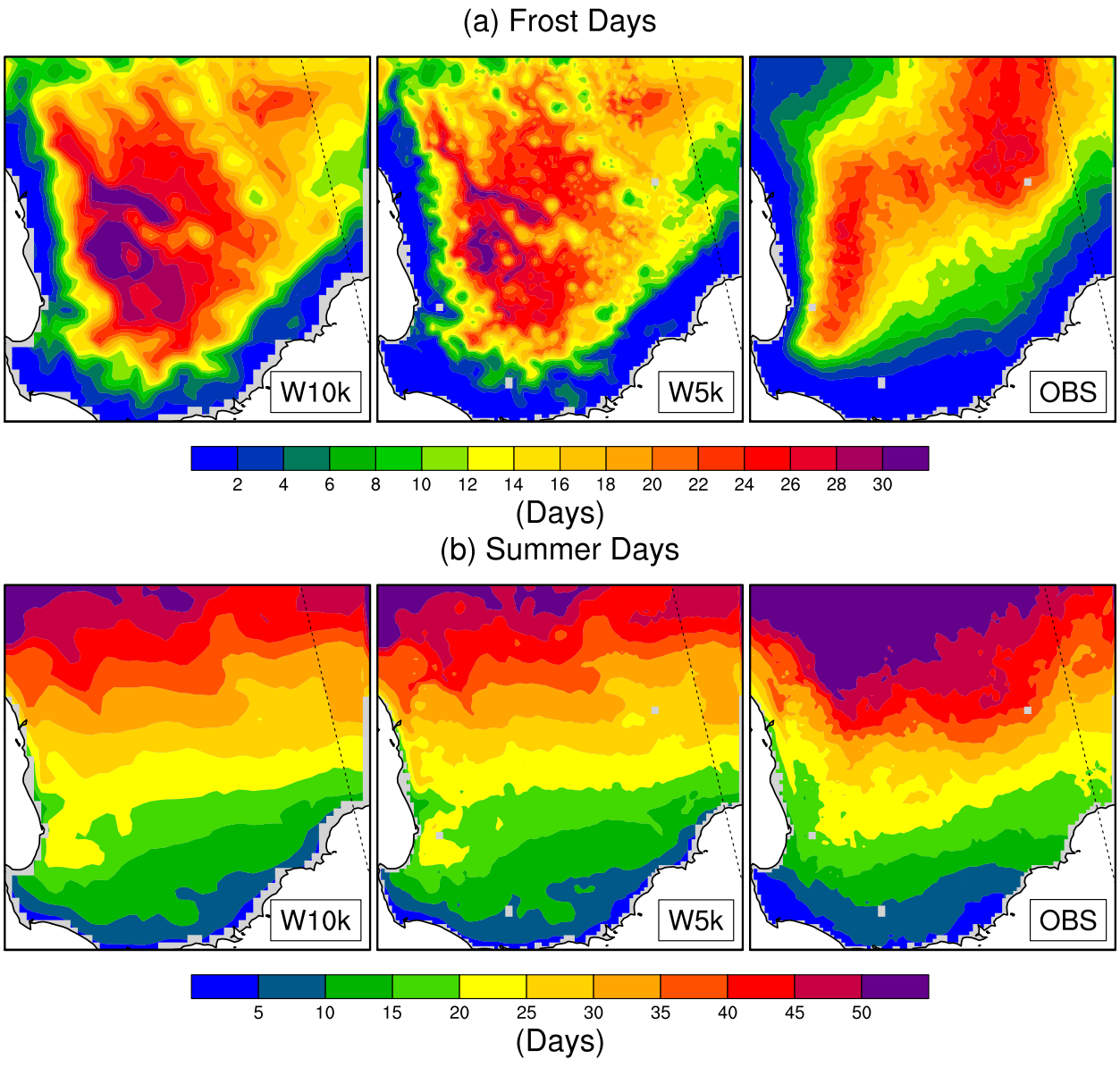

FIG. 17. Values of the temperature indices (a) FD and (b) SU for W10k, W5k, and observations.

downscaling ratio between the two domains compared in Soares et al. (2012) was 3, whereas the downscaling ratio used in our research was 2.

It was expected that the W5k simulation would demonstrate improved results when compared with W10k, but this finding was equivocal. W5k is influenced by edge effects in the southwestern coastal regions but even removing these affected areas from our analysis does not always elevate the performance of the W5k simulation above that of W10k. For example, W10k provided a better representation of R95pTOT and SDII relative to W5k in the interior of the domain. Despite the fact that the performance of W5k is not always superior to W10k, this high-resolution model does consistently demonstrate improved simulation skill with respect to convective precipitation, rainfall surrounding the Darling Scarp, and also frost.

For applications related to cereal-crop production in SWWA, the W5k simulation is useful because it reduces the negative JJA rainfall bias in the interior of the domain, which is the area of main agricultural production in the region. Furthermore, representation of the daily distribution of precipitation is improved significantly by the higher-resolution simulation, which indicates that the W5k simulation is providing a better

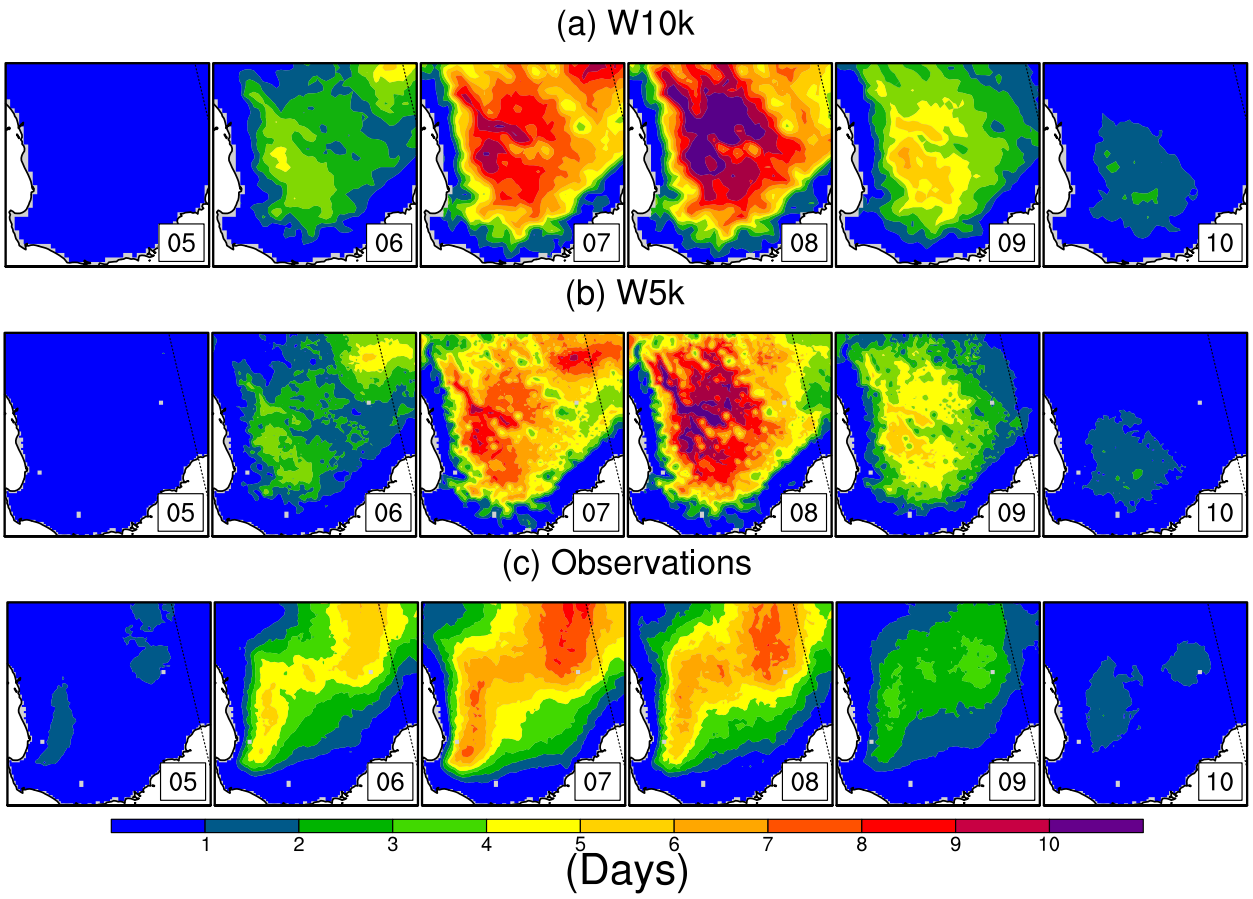

FIG. 18. Monthly (05–10 = May–October) values of FD over the growing season for (a) W10k, (b) W5k, and (c) observations.

spatial representation of rainfall. W5k does not show as marked an improvement on temperature representation, and this result is because temperatures, particularly maxima, are not as heavily affected by the finer-scale features that the higher-resolution domain improves upon. When we consider the temporal distributions of the SU and FD indices in accordance with the growing season, however, we do see that, for both metrics, W5k improves the spatiotemporal representation of these indices relative to W10k.

There are a number of regional climate studies that demonstrate improved simulation performance when comparing domains of 30–50 km with domains of 9–15 km in which both domains employ convective parameterization (Cardoso et al. 2013; Soares et al. 2012; Heikkilä et al. 2011). Fewer studies compare a 10-km domain with a higher-resolution grid that is explicitly resolving convection. Villarroel et al. (2013) found that a high-resolution 5-km domain over southern Chile improved model performance for both temperature and precipitation relative to the driving data, and this result was attributed to improved topographical resolution, but the domain was not compared with a lower-resolution WRF grid. In a simulation over central Japan, Kusaka et al. (2010) found that 4-km resolution represented a 5-yr climatology well; again, these results were compared with a lower-resolution WRF grid. Warrach-Sagi et al. (2013) conducted a 30-yr simulation over Germany at 10-km resolution and then compared these results with a shorter, convection-resolving simulation at 5-km resolution. Their findings were consistent with our own in demonstrating that a convection-resolving resolution can overcome the windward/lee effect that is apparent at 10-km resolution (W10k), and they support the use of high-resolution, convection-resolving simulations for RCM.

On the basis of the results of W10k and W5k, particularly the spatial and temporal representation of the climate extremes that were considered in this research, we have high confidence in the model for regional climate simulations over SWWA.

Acknowledgments. This research was supported by an Australian Grains Research and Development

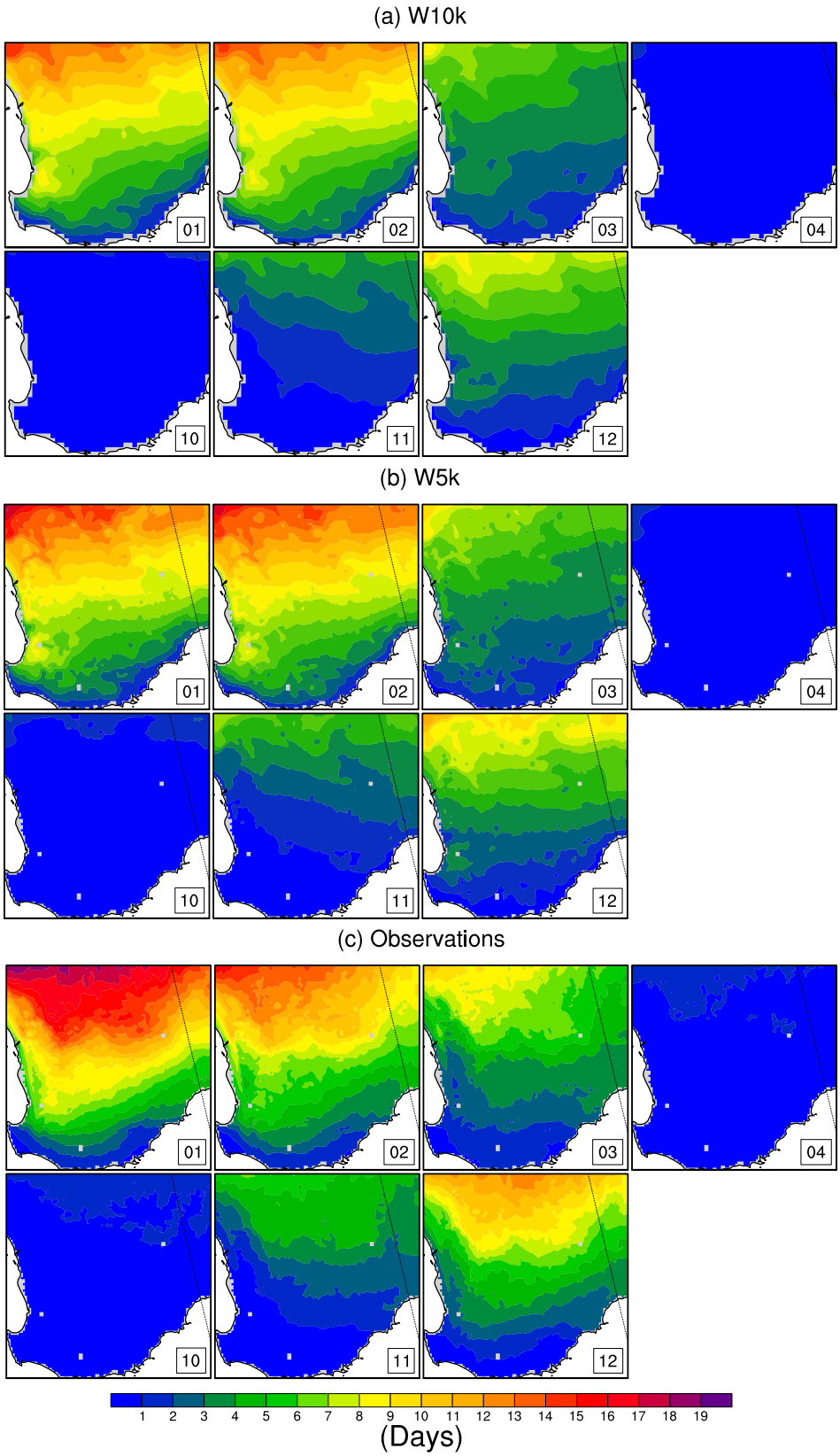

FIG. 19. Monthly (01–04 = January–April; 10–12 = October–December) values of SU for (a) W10k, (b) W5k, and (c) observations.

Corporation (GRDC) Grant (MCV0013). Julia Andrys is supported by an Australian Postgraduate Award and a GRDC Top Up Scholarship. Jatin Kala is supported by the Australian Research Council Centre of Excellence for Climate Systems Science (CE110001028). The research group led by Associate Professor Jason Evans at the University of New South Wales, Australia, provided the modified version of WRFv3.3 used in this study and assisted in the preprocessing of the input data. Computational modeling was supported by iVEC through the use of advanced computing resources provided by the Pawsey Super Computing Centre located at iVec@Murdoch. It was funded under the National Computational Merit Allocation Scheme and the iVec Partner Allocation Scheme. All of this support is gratefully acknowledged. The authors also thank the two anonymous reviewers whose comments helped to improve this manuscript.

REFERENCES

Allen, C. D., and Coauthors, 2010: A global overview of drought and heat-induced tree mortality reveals emerging climate change risks for forests. *For. Ecol. Manage.,* **259,** 660–684, doi:10.1016/j.foreco.2009.09.001.

Argüeso, D., J. M. Hidalgo-Muñoz, S. R. Gámiz-Fortis, M. J. Esteban-Parra, J. Dudhia, and Y. Castro-Díez, 2011: Evaluation of WRF parameterizations for climate studies over southern Spain using a multistep regionalization. *J. Climate,* **24,** 5633–5651, doi:10.1175/JCLI-D-11-00073.1.

——, ——, ——, ——, and Y. Castro-Díez, 2012: Evaluation of WRF mean and extreme precipitation over Spain: Present climate (1970–99). *J. Climate,* **25,** 4883–4897, doi:10.1175/JCLI-D-11-00276.1.

Asseng, S., I. Foster, and N. C. Turnder, 2011: The impact of temperature variability on wheat yields. *Global Change Biol.,* **17,** 997–1012, doi:10.1111/j.1365-2486.2010.02262.x.

——, D. Thomas, P. McIntosh, O. Alves, and N. Khimashia, 2012: Managing mixed wheat–sheep farms with a seasonal forecast. *Agric. Syst.,* **113,** 50–56, doi:10.1016/j.agsy.2012.08.001.

Brouwers, N. C., J. Mercer, T. Lyons, P. Poot, E. Veneklaas, and G. Hardy, 2012: Climate and landscape drivers of tree decline in a Mediterranean ecoregion. *Ecol. Evol.,* **3,** 67–79, doi:10.1002/ece3.437.

Cardoso, R. M., P. M. M. Soares, P. M. A. Miranda, and M. BeloPereira, 2013: WRF high resolution simulation of Iberian mean and extreme precipitation climate. *Int. J. Climatol.,* **33,** 2591–2608, doi:10.1002/joc.3616.

Chen, F., and J. Dudhia, 2001: Coupling an advanced land surface–hydrology model with the Penn State–NCAR MM5 modeling system. Part I: Model implementation and sensitivity. *Mon. Wea. Rev.,* **129,** 569–585, doi:10.1175/1520-0493(2001)129<0569:CAALSH>2.0.CO;2.

——, and Coauthors, 2011: The integrated WRF/urban modelling system: Development, evaluation, and applications to urban environmental problems. *Int. J. Climatol.,* **31,** 273–288, doi:10.1002/joc.2158.

Chotamonsak, C., E. P. Salathé Jr., J. Kreasuwan, S. Chantara, and K. Siriwitayakorn, 2011: Projected climate change over Southeast Asia simulated using a WRF regional climate model. *Atmos. Sci. Lett.,* **12,** 213–219, doi:10.1002/asl.313.

Christensen, J. H., T. R. Carter, M. Rummukainen, and G. Amanatidis, 2007: Evaluating the performance and utility of regional climate models: The PRUDENCE project. *Climatic Change,* **81,** 1–6, doi:10.1007/s10584-006-9211-6.

Chu, J., K. Warrach-Sagi, V. Wulfmeyer, T. Schwitalla, and H. Bauer, 2010: Regional climate simulation (1989-2009) with WRF in the CORDEX-Europe domain. *Abstracts, 10th EMS Annual Meeting and 8th European Conf. on Applied Climatology (ECAC),* Zürich, Switzerland, European Meteorological Society, EMS2010-209. [Available online at http://meetingorganizer.copernicus.org/EMS2010/EMS2010-209-1.pdf.]

Clifford, M. J., P. D. Royer, N. S. Cobb, D. D. Breshears, and P. L. Ford, 2013: Precipitation thresholds and drought-induced tree die-off: Insights from patterns of *Pinus edulis* mortality along an environmental stress gradient. *New Phytol.,* **200,** 413–421, doi:10.1111/nph.12362.

Dee, D. P., and Coauthors, 2011: The ERA-Interim reanalysis: Configuration and performance of the data assimilation system. *Quart. J. Roy. Meteor. Soc.,* **137,** 553–597, doi:10.1002/qj.828.

Donat, M. G., G. C. Leckebusch, J. G. Pinto, and U. Ulbrich, 2010: European storminess and associated circulation weather types: Future changes deduced from a multi-model ensemble of GCM simulations. *Climate Res.,* **42,** 27–43, doi:10.3354/cr00853.

Dudhia, J., 1989: Numerical study of convection observed during the Winter Monsoon Experiment using a mesoscale two-dimensional model. *J. Atmos. Sci.,* **46,** 3077–3107, doi:10.1175/1520-0469(1989)046<3077:NSOCOD>2.0.CO;2.

Easterling, D. R., G. A. Meehl, C. Parmesan, S. A. Changnon, T. R. Karl, and L. O. Mearns, 2000: Climate extremes: Observations, modeling, and impacts. *Science,* **289,** 2068–2074, doi:10.1126/science.289.5487.2068.

Ekström, M., H. J. Fowler, C. G. Kilsby, and P. D. Jones, 2005: New estimates of future changes in extreme rainfall across the UK using regional climate model integrations. 2. Future estimates and use in impact studies. *J. Hydrol.,* **300,** 234–251, doi:10.1016/j.jhydrol.2004.06.019.

England, M. H., C. C. Ummenhofer, and A. Santoso, 2006: Interannual rainfall extremes over southwest Western Australia linked to Indian Ocean climate variability. *J. Climate,* **19,** 1948–1969, doi:10.1175/JCLI3700.1.

Evans, B., and T. Lyons, 2013: Bioclimatic extremes drive forest mortality in southwest, Western Australia. *Climate,* **1** (2), 28–52, doi:10.3390/cli1020028.

Evans, J. P., and M. F. McCabe, 2010: Regional climate simulation over Australia's Murray-Darling basin: A multitemporal assessment. *J. Geophys. Res.,* **115,** D14114, doi:10.1029/2010JD013816.

——, M. Ekström, and F. Ji, 2012: Evaluating the performance of a WRF physics ensemble over south-east Australia. *Climate Dyn.,* **39,** 1241–1258, doi:10.1007/s00382-011-1244-5.

Fitzpatrick, M. C., A. D. Gove, N. J. Sanders, and R. R. Dunn, 2008: Climate change, plant migration, and range collapse in a global biodiversity hotspot: The Banksia (Proteaceae) of Western Australia. *Global Change Biol.,* **14,** 1337–1352, doi:10.1111/j.1365-2486.2008.01559.x.

Fowler, H. J., M. Ekström, C. G. Kilsby, and P. D. Jones, 2005: New estimates of future changes in extreme rainfall across the UK using regional climate model integrations. 1. Assessment of control climate. *J. Hydrol.,* **300,** 212–233, doi:10.1016/j.jhydrol.2004.06.017.

Gao, Y., J. S. Fu, J. B. Drake, Y. Liu, and J. F. Lamarque, 2012: Projected changes of extreme weather events in the eastern United States based on a high resolution climate modeling system. *Environ. Res. Lett.,* **7,** 044025, doi:10.1088/1748-9326/7/4/044025.

Gentilli, J., 1971: *Climates of Australia and New Zealand*. Elsevier, 405 pp.

Giorgi, F., C. Jones, and G. R. Asrar, 2009: Addressing climate information needs at the regional level: The CORDEX framework. *WMO Bull.,* **58,** 175–183. [Available online at https://www.wmo.int/pages/publications/bulletin_en/archive/58_3_en/documents/58_3_giorgi_en.pdf.]

Grell, G. A., S. Emeis, W. R. Stockwell, T. Schoenemeyer, R. Forkel, J. Michalakes, R. Knoche, and W. Seidl, 2000: Application of a multiscale, coupled MM5/chemistry model to the complex terrain of the VOTALP valley campaign. *Atmos. Environ.,* **34,** 1435–1453, doi:10.1016/S1352-2310(99)00402-1.

Heikkilä, U., A. Sandvik, and A. Sorteberg, 2011: Dynamical downscaling of ERA-40 in complex terrain using the WRF regional climate model. *Climate Dyn.,* **37,** 1551–1564, doi:10.1007/s00382-010-0928-6.

Hong, S.-Y., and J.-O. J. Lim, 2006: The WRF single-moment 6-class microphysics scheme (WSM6). *J. Korean Meteor. Soc.,* **42,** 129–151.

——, J. Dudhia, and S.-H. Chen, 2004: A revised approach to ice microphysical processes for the bulk parameterization of clouds and precipitation. *Mon. Wea. Rev.,* **132,** 103–120, doi:10.1175/1520-0493(2004)132<0103:ARATIM>2.0.CO;2.

Hughes, L., 2003: Climate change and Australia: Trends, projections and impacts. *Austral Ecol.,* **28,** 423–443, doi:10.1046/j.1442-9993.2003.01300.x.

Jones, D. A., W. Wang, and R. Fawcett, 2009: High-quality spatial climate data-sets for Australia. *Aust. Meteor. Oceanogr. J.,* **58,** 233–248.

Kain, J. S., 2004: The Kain–Fritsch convective parameterization: An update. *J. Appl. Meteor.,* **43,** 170–181, doi:10.1175/1520-0450(2004)043<0170:TKCPAU>2.0.CO;2.

Kala, J., T. J. Lyons, I. J. Foster, and U. S. Nair, 2009: Validation of a simple steady-state forecast of minimum nocturnal temperatures. *J. Appl. Meteor. Climatol.,* **48,** 624–633, doi:10.1175/2008JAMC1956.1.

——, ——, and U. S. Nair, 2011: Numerical simulations of the impacts of land-cover change on cold fronts in south-west Western Australia. *Bound.-Layer Meteor.,* **138,** 121–138, doi:10.1007/s10546-010-9547-3.

——, J. Andrys, T. J. Lyons, I. J. Foster, and B. Evans, 2015: Sensitivity of WRF to driving data and physics options on a seasonal time-scale for the southwest of Western Australia. *Climate Dyn.,* doi:10.1007/s00382-014-2160-2, in press.

Keeling, C. D., S. C. Piper, R. B. Bacastow, M. Wahlen, T. P. Whorf, M. Heimann, and H. A. Meijer, 2001: Exchanges of atmospheric CO_2 and $^{13}CO_2$ with the terrestrial biosphere and oceans from 1978 to 2000. I. Global aspects. SIO Reference Series Tech. Rep. 01-06, 28 pp. [Available online at http://scrippsco2.ucsd.edu/publications/keeling_sio_ref_series_exchanges_of_co2_ref_no_01-06_2001.pdf.]

King, A. D., L. V. Alexander, and M. G. Donat, 2013: The efficacy of using gridded data to examine extreme rainfall characteristics: A case study for Australia. *Int. J. Climatol.,* **33,** 2376–2387, doi:10.1002/joc.3588.

Kingwell, R., 2006: Climate change in Australia: Agricultural impacts and adaptation. *Austr. Agribus. Rev.,* **14,** Paper 1, 29 pp. [Available online at http://www.agrifood.info/review/2006/Kingwell.pdf.]

Kusaka, H., T. Takata, and Y. Takane, 2010: Reproducibility of regional climate in central Japan using the 4-km resolution WRF Model. *SOLA,* **6,** 113–116, doi:10.2151/sola.2010-029.

Lowrey, M. R. K., and Z.-L. Yang, 2008: Assessing the capability of a regional-scale weather model to simulate extreme precipitation patterns and flooding in central Texas. *Wea. Forecasting,* **23,** 1102–1126, doi:10.1175/2008WAF2006082.1.

Ludwig, F., and S. Asseng, 2006: Climate change impacts on wheat production in a Mediterranean environment in Western Australia. *Agric. Syst.,* **90,** 159–179, doi:10.1016/j.agsy.2005.12.002.

Malcolm, J. R., C. Liu, R. P. Neilson, L. Hansen, and L. E. E. Hannah, 2006: Global warming and extinctions of endemic species from biodiversity hotspots. *Conserv. Biol.,* **20,** 538–548, doi:10.1111/j.1523-1739.2006.00364.x.

Mearns, L. O., W. Gutowski, R. Jones, R. Leung, S. McGinnis, A. Nunes, and Y. Qian, 2009: A regional climate change assessment program for North America. *Eos, Trans. Amer. Geophys. Union,* **90** (36), 311–312, doi:10.1029/2009EO360002.

Mishra, V., F. Dominguez, and D. P. Lettenmaier, 2012: Urban precipitation extremes: How reliable are regional climate models? *Geophys. Res. Lett.,* **39,** L03407, doi:10.1029/2011GL050658.

Mlawer, E. J., S. J. Taubman, P. D. Brown, M. J. Iacono, and S. A. Clough, 1997: Radiative transfer for inhomogeneous atmospheres: RRTM, a validated correlated-*k* model for the longwave. *J. Geophys. Res.,* **102,** 16 663–16 682, doi:10.1029/97JD00237.

Niu, S., Y. Luo, D. Li, S. Cao, J. Xia, J. Li, and M. D. Smith, 2014: Plant growth and mortality under climatic extremes: An overview. *Environ. Exp. Bot.,* **98,** 13–19, doi:10.1016/j.envexpbot.2013.10.004.

Patricola, C. M., and K. H. Cook, 2013: Mid-twenty-first century warm season climate change in the central United States. Part I: Regional and global model predictions. *Climate Dyn.,* **40,** 551–568, doi:10.1007/s00382-012-1605-8.

Patz, J. A., D. Campbell-Lendrum, T. Holloway, and J. A. Foley, 2005: Impact of regional climate change on human health. *Nature,* **438,** 310–317, doi:10.1038/nature04188.

Perkins, S. E., A. J. Pitman, N. J. Holbrook, and J. McAneney, 2007: Evaluation of the AR4 climate models simulated daily maximum temperature, minimum temperature, and precipitation over Australia using probability density functions. *J. Climate,* **20,** 4356–4376, doi:10.1175/JCLI4253.1.

Persson, G., L. Bärring, E. Kjellström, G. Strandberg, and M. Rummukainen, 2007: Climate indices for vulnerability assessments. Swedish Meteorological and Hydrological Institute Meteorology and Climatology Rep. (RMK) 111, 80 pp. [Available online at http://www.smhi.se/polopoly_fs/1.805!Climate%20indices%20for%20vulnerability%20assessments.pdf.]

Pitts, R. O., and T. J. Lyons, 1990: Airflow over a two-dimensional escarpment. II: Hydrostatic flow. *Quart. J. Roy. Meteor. Soc.,* **116,** 363–378, doi:10.1002/qj.49711649207.

Pook, M. J., J. S. Risbey, and P. C. McIntosh, 2012: The synoptic climatology of cool-season rainfall in the central wheatbelt of Western Australia. *Mon. Wea. Rev.,* **140,** 28–43, doi:10.1175/MWR-D-11-00048.1.

Power, S., F. Tseitkin, S. Torok, B. Lavery, R. Dahni, and B. Mcavaney, 1998: Australian temperature, Australian rainfall and the Southern Oscillation, 1910–1992: Coherent variability and recent changes. *Aust. Meteor. Mag.,* **47,** 85–101.

Raupach, M. R., P. R. Briggs, V. Haverd, E. A. King, M. Paget, and C. M. Trudinger, 2009: Australian Water Availability Project (AWAP): CSIRO Marine and Atmospheric Research Component: Final Report for Phase 3. CAWCR Tech. Rep. 013,

67 pp. [Available online at http://www.csiro.au/awap/doc/CTR_013_online_FINAL.pdf.]

Salathé, E. P., L. R. Leung, Y. Qian, and Y. Zhang, 2010: Regional climate model projections for the state of Washington. *Climatic Change,* **102,** 51–75, doi:10.1007/s10584-010-9849-y.

Seth, A., and F. Giorgi, 1998: The effects of domain choice on summer precipitation simulation and sensitivity in a regional climate model. *J. Climate,* **11,** 2698–2712, doi:10.1175/1520-0442(1998)011<2698:TEODCO>2.0.CO;2.

Skamarock, W. C., and Coauthors, 2008: A description of the Advanced Research WRF version 3. NCAR Tech. Note NCAR/TN-475+STR, 113 pp. [Available online at http://www.mmm.ucar.edu/wrf/users/docs/arw_v3_bw.pdf.]

Soares, P. M. M., R. M. Cardoso, P. M. A. Miranda, J. Medeiros, M. Belo-Pereira, and F. Espirito-Santo, 2012: WRF high resolution dynamical downscaling of ERA-Interim for Portugal. *Climate Dyn.,* **39,** 2497–2522, doi:10.1007/s00382-012-1315-2.

Tapp, R. G., and S. L. Barrell, 1984: The northwest Australian cloud band: Climatology, characteristics and factors associated with development. *J. Climatol.,* **4,** 411–424, doi:10.1002/joc.3370040406.

Taylor, K. E., 2001: Summarizing multiple aspects of model performance in a single diagram. *J. Geophys. Res.,* **106,** 7183–7192, doi:10.1029/2000JD900719.

Varnas, D., cited 2014: Western Australian grains industry. [Available online at https://www.agric.wa.gov.au/grains-research-development/western-australian-grains-industry.]

Villarroel, C., J. F. Carrasco, G. Casassa, and M. Falvey, 2013: Modeling near-surface air temperature and precipitation using WRF with 5-km resolution in the northern Patagonia icefield: A pilot simulation. *Int. J. Geosci.,* **4,** 1193–1199, doi:10.4236/ijg.2013.48113.

Wardlaw, I. F., 1994: The effect of high temperature on kernel development in wheat: Variability related to pre-heading and post-anthesis conditions. *Aust. J. Plant Physiol.,* **21,** 731–739, doi:10.1071/PP9940731.

Warrach-Sagi, K., T. Schwitalla, V. Wulfmeyer, and H.-S. Bauer, 2013: Evaluation of a climate simulation in Europe based on the WRF–Noah model system: Precipitation in Germany. *Climate Dyn.,* **41,** 755–774, doi:10.1007/s00382-013-1727-7.

Williams, A. P., and Coauthors, 2012: Temperature as a potent driver of regional forest drought stress and tree mortality. *Nat. Climate Change,* **3,** 292–297, doi:10.1038/nclimate1693.

Wright, P. B., 1974: Seasonal rainfall in southwestern Australia and the general circulation. *Mon. Wea. Rev.,* **102,** 219–232, doi:10.1175/1520-0493(1974)102<0219:SRISAA>2.0.CO;2.

Wulfmeyer, V., and Coauthors, 2008: The Convective and Orographically Induced Precipitation Study: A research and development project of the World Weather Research Program for improving quantitative precipitation forecasting in low-mountain regions. *Bull. Amer. Meteor. Soc.,* **89,** 1477–1486, doi:10.1175/2008BAMS2367.1.

Zhang, Y., V. Dulière, P. W. Mote, and E. P. Salathé, 2009: Evaluation of WRF and HadRM mesoscale climate simulations over the U.S. Pacific Northwest. *J. Climate,* **22,** 5511–5526, doi:10.1175/2009JCLI2875.1.

Zheng, B., K. Chenu, M. Fernanda Dreccer, and S. C. Chapman, 2012: Breeding for the future: What are the potential impacts of future frost and heat events on sowing and flowering time requirements for Australian bread wheat (*Triticum aestivium*) varieties? *Global Change Biol.,* **18,** 2899–2914, doi:10.1111/j.1365-2486.2012.02724.x.